

Surfactant Protein B Promotes Cytosolic siRNA Delivery by Adopting a Virus-like Mechanism of Action

Roberta Guagliardo, Lore Herman, Jelle Penders, Agata Zamborlin, Herlinde De Keersmaecker, Thijs Van de Vyver, Sandrine Verstraeten, Pieterjan Merckx, Marie-Paule Mingeot-Leclercq, Mercedes Echaide, Jesús Pérez-Gil, Molly M. Stevens, Stefaan C. De Smedt, and Koen Raemdonck*



Cite This: *ACS Nano* 2021, 15, 8095–8109



Read Online

ACCESS |



Metrics & More



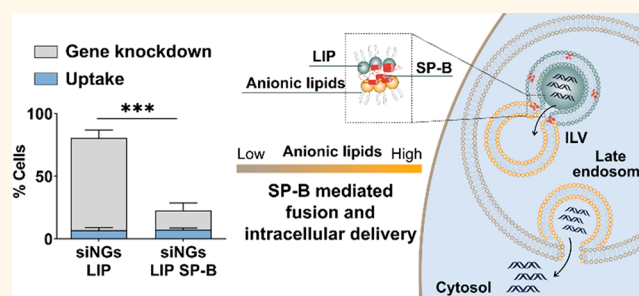
Article Recommendations



Supporting Information

ABSTRACT: RNA therapeutics are poised to revolutionize medicine. To unlock the full potential of RNA drugs, safe and efficient (nano)formulations to deliver them inside target cells are required. Endosomal sequestration of nanocarriers represents a major bottleneck in nucleic acid delivery. Gaining more detailed information on the intracellular behavior of RNA nanocarriers is crucial to rationally develop delivery systems with improved therapeutic efficiency. Surfactant protein B (SP-B) is a key component of pulmonary surfactant (PS), essential for mammalian breathing. In contrast to the general belief that PS should be regarded as a barrier for inhaled nanomedicines, we recently discovered the ability of SP-B to promote gene silencing by siRNA-loaded and lipid-coated nanogels. However, the mechanisms governing this process are poorly understood. The major objective of this work was to obtain mechanistic insights into the SP-B-mediated cellular delivery of siRNA. To this end, we combined siRNA knockdown experiments, confocal microscopy, and focused ion beam scanning electron microscopy imaging in an *in vitro* non-small-cell lung carcinoma model with lipid mixing assays on vesicles that mimic the composition of (intra)cellular membranes. Our work highlights a strong correlation between SP-B-mediated fusion with anionic endosomal membranes and cytosolic siRNA delivery, a mode of action resembling that of certain viruses and virus-derived cell-penetrating peptides. Building on these gained insights, we optimized the SP-B proteolipid composition, which dramatically improved delivery efficiency. Altogether, our work provides a mechanistic understanding of SP-B-induced perturbation of intracellular membranes, offering opportunities to fuel the rational design of SP-B-inspired RNA nanoformulations for inhalation therapy.

KEYWORDS: nanomedicine, siRNA, cellular delivery, pulmonary surfactant, nano–bio interface, endosomal escape



In the last two decades, the application of small interfering RNA (siRNA) therapeutics has gained considerable interest, as it allows the treatment of virtually any human disease. siRNAs can be designed to induce mRNA degradation with high specificity, allowing a precise and effective knockdown of the expression of particular disease-related genes.¹ Since the discovery of the RNA interference (RNAi) mechanism and the recognition of its therapeutic value, many researchers have focused their attention on the development of suitable formulations to safely and effectively deliver this type of therapeutic agent into target cells. The need for a delivery system is imposed by the many extra- and intracellular barriers that an siRNA drug encounters upon *in vivo* administration.^{2,3} At the intracellular level, siRNAs need to be delivered into the cytosol of the target cells to exert their

gene silencing function *via* activation of the RNAi machinery.⁴ Different types of nanosized carriers, both viral and nonviral, have been investigated for this purpose.^{5,6} Although viral vectors enable efficient intracellular delivery *via* the exploitation of specific cell infection pathways,⁷ they show an unfavorable safety profile due to the risk of insertional mutagenesis and immunogenicity.⁸ Moreover, their use is limited by high costs and difficulties to expand their

Received: May 29, 2020

Accepted: March 8, 2021

Published: March 16, 2021



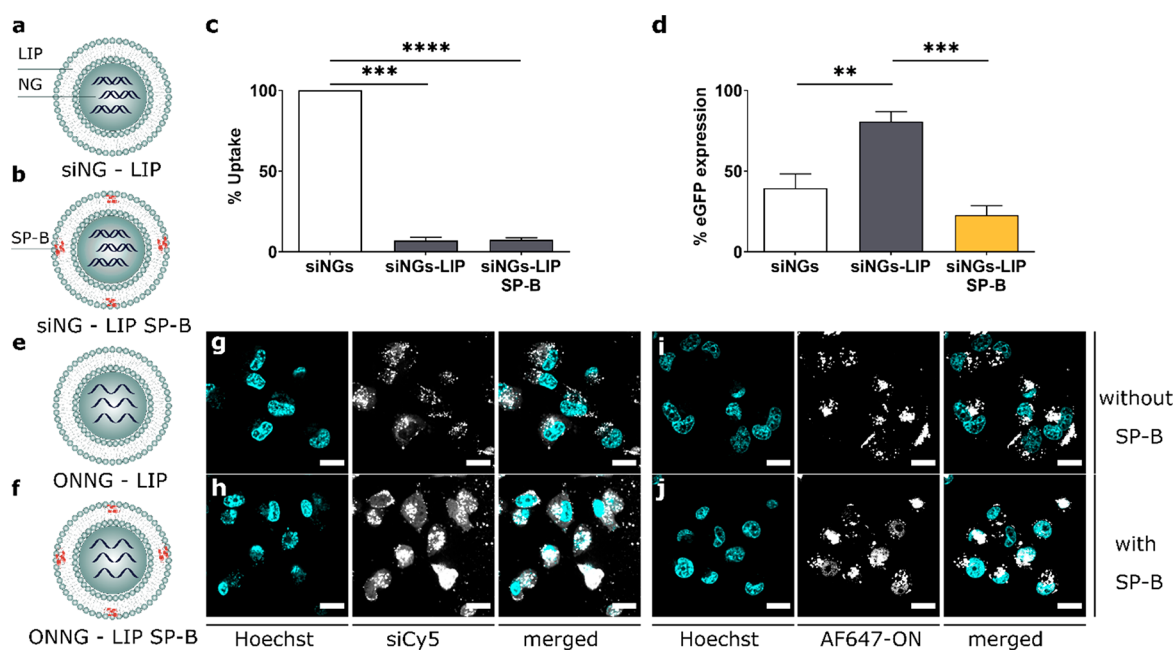


Figure 1. Evaluation of SP-B-mediated cytosolic delivery of siRNA and single-stranded oligonucleotides (ONs). (a, b, e, f) Visual representations of the PS-inspired (proteo)lipid-coated nanogel structures. Dextran nanogels (NGs), (a, b) siRNA-loaded (siNGs), or (e, f) ON-loaded NGs (ONNGs) are coated with a lipid mixture of DOPC:PG (85:15 wt %) (LIP) with or without SP-B (0.4 wt %). Flow cytometric quantification of (c) Cy5-labeled siRNA (siCys5) cellular uptake and (d) eGFP gene knockdown of coated and uncoated siNGs, in H1299_eGFP cells. Data are represented as mean \pm standard deviation (SD) of three independent repeats (statistical analysis was performed using one-way ANOVA, $**p \leq 0.01$, $***p \leq 0.001$, $****p \leq 0.0001$). (g) Representative confocal microscopy images of nuclei (cyan) and siCys5 (gray) accumulation in the endosomes (punctuate pattern), when formulated in siNGs-LIP and (h) both punctuate pattern and siCys5 diffuse staining of the cytoplasm when SP-B is present in the lipid coating. (i) Representative confocal microscopy images of nuclei (cyan) and Alexa Fluor-647 ON (ON) (gray) accumulation in the endosomes (punctuate pattern) when formulated in ONNG-LIP and (j) both punctuate pattern and ON cytosolic delivery followed by nuclear accumulation when SP-B is present in the lipid coating. Scale bars in the confocal images indicate 20 μm .

production on an industrial scale.⁹ Contrarily, nonviral vectors have gained significant interest because of their ease of manufacture and flexible design, as a result of the wide variety of applicable materials and engineering approaches.⁶ The recent approval of the siRNA-based medicinal products Onpatro (patisiran) and Givlaari (givosiran), *i.e.*, a lipid nanoparticle (LNP) and a GalNAc-conjugate, respectively, designed for siRNA delivery to liver cells, represents an important milestone for the siRNA delivery field.¹⁰ However, even for these state-of-the-art formulations, cytosolic delivery remains relatively inefficient. LNPs are typically taken up by cells through endocytosis, sequestering the therapeutic cargo into endocytic compartments, which necessitates endosomal escape for functional siRNA delivery. Recent studies have indicated that endosomal escape still represents one of the main bottlenecks in cytosolic delivery of RNA, with only 1–2% of the endocytosed RNA dose actually reaching the cytosol.^{11–14} These insights underscore the need for effective materials to enhance the endosomal escape of RNA therapeutics.

We recently reported on the repurposing of a clinically approved pulmonary surfactant (PS), *i.e.*, poractant alfa (Curosurf), for drug delivery purposes. Although generally applied as surfactant replacement therapy to treat respiratory distress syndrome in preterm infants, De Backer *et al.* described the use of Curosurf as a biomaterial to promote RNAi.^{15–20} More specifically, layering siRNA-loaded biodegradable dextran nanogels with Curosurf improved both their

colloidal stability and siRNA-induced target gene knockdown efficiency *in vitro* and *in vivo*.¹⁸

PS is a complex mixture of lipids and proteins that plays an essential role in surface tension dynamics at the alveolar air–liquid interface.²¹ Secreted by alveolar type II cells, its lipid fraction (~ 90 wt %) includes mainly zwitterionic phosphatidylcholine (PC) (~ 70 wt %), anionic phosphatidylglycerol (PG) (~ 10 wt %), and neutral lipids, the latter being mostly cholesterol (~ 8 wt %).²² The remaining surfactant fraction is composed of two classes of surfactant proteins (SPs), the hydrophilic SP-A and SP-D and the hydrophobic SP-B and SP-C.²³ While the larger hydrophilic SPs mainly have a role in the innate immune system and therefore are removed from the clinical preparations,^{24–26} their smaller hydrophobic counterparts play an essential role in surface tension reduction.^{27–30} PS dynamics at the alveolar interface have been investigated from both a biophysical and clinical point of view.^{31–33} In the drug delivery field, however, PS is usually considered as an additional extracellular barrier following pulmonary administration.³⁴ The formation of a biomolecular surfactant corona might hinder the direct interaction between NPs and cellular membranes as well as induce NP aggregation and premature cargo release.^{35,36} In contrast to this paradigm, having established PS as a delivery-promoting biomaterial, we recently identified the cationic amphiphilic protein SP-B as the key component of PS responsible for improved siRNA-induced gene knockdown.¹⁹ Although lipid membrane-perturbing effects of SP-B have been described to explain the stabilization of alveolar surfactant films during repetitive breathing cycles,

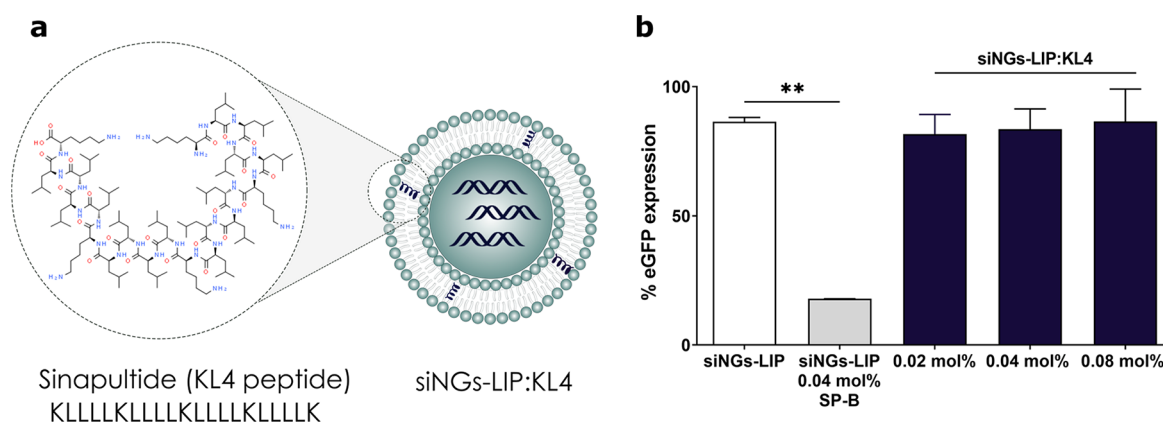


Figure 2. Evaluation of gene knockdown efficiency of KL4 as synthetic replacement of SP-B. (a) Visual representation of the PS-inspired (proteo)lipid-coated nanogel structure including the synthetic peptide KL4 (sinapultide) instead of the full native protein SP-B. (b) Gene knockdown potential of siNGs coated with LIP or with LIP supplemented with SP-B or KL4 at the indicated mol %. Data are represented as mean \pm SD of two independent repeats (statistical analysis was performed using one-way ANOVA, $**p \leq 0.01$).

its cellular mechanism of action underlying the enhanced gene silencing effect remains obscure. In this work, we combined *in cellulo* transfection experiments as well as confocal and electron microscopy imaging in a non-small-cell lung cancer cell model with *in vitro* lipid mixing assays to gain mechanistic insight into the cellular behavior of SP-B. First, our data revealed that formulating SP-B into lipid-coated nanocomposites allows cytosolic delivery of fluorescently labeled siRNA and single-stranded oligonucleotides (ONs), an effect requiring direct contact with cellular membranes. More specifically, we could show that low fractions of the cationic SP-B promote fusion with negatively charged endosomal membranes, in contrast to its cationic and amphiphilic counterpart SP-C and the SP-B mimicking peptide KL4. Finally, guided by these acquired insights, we were able to strongly promote the siRNA delivery potential of the above-mentioned nanocomposites through a minor reduction of the anionic charge density of the lipid coat.

RESULTS AND DISCUSSION

SP-B Enhances Cytosolic Delivery of Small Nucleic Acids via Proteolipid-Coated Nanogels. We previously showed enhanced gene silencing using siRNA-loaded PS-coated nanogels both *in vitro* and *in vivo*.^{16–18} The beneficial effect of PS was investigated in more detail by Merckx *et al.*, who identified the cationic amphiphilic surfactant protein B (SP-B) as a key component of lung surfactant involved in improved gene knockdown.¹⁹ Further optimizations led to the formulation of a PS-inspired proteolipid-coated nanocomposite consisting of an siRNA-loaded nanogel core (siNG) surrounded by a lipid layer (LIP) composed of DOPC:PG (85:15 wt %) and supplemented with 0.4 wt % of SP-B (Figure 1a and b).¹⁹ As demonstrated earlier, even though the lipid coat reduced the intracellular siRNA dose by $\sim 90\%$ (Figure 1c), the addition of physiological fractions of SP-B to the lipid bilayer generated levels of silencing comparable to the uncoated formulation in H1299_eGFP cells (Figure 1d). This effect could not be explained by SP-B-promoted cellular uptake, as both formulations reached equal intracellular siRNA levels (Figure 1c). Moreover, a similar gradual decrease in cellular siRNA dose was noted as a function of time post-transfection, independent of SP-B (Supporting Figure 1). To assess a potential impact of SP-B on the endocytic uptake mechanism, cells were exposed to mounting concentrations of

three well-known endocytic inhibitors.^{37,38} Pronounced reduction of cellular uptake was mainly observed for chlorpromazine and 5-(*N*-ethyl-*N*-isopropyl)amiloride (EIPA), indicating the involvement of both clathrin-mediated endocytosis and macropinocytosis in the uptake process, respectively. Importantly, both siNGs-LIP and siNGs-LIP SP-B again performed similarly, suggesting that the presence of SP-B in the proteolipid coat of the nanogels does not have a major impact on the endocytic uptake process (Supporting Figure 1). Considering that SP-B neither enhances the cellular uptake of the nanocomposites nor impacts the exploited endocytic route, we hypothesized that SP-B could rather improve the cytosolic delivery of the encapsulated siRNA at the level of the endosomes.^{19,20} The cells treated with the lipid-coated formulation (siNGs-LIP) only showed a punctuate pattern of Cy5-labeled siRNA, indicating accumulation in endosomal/lysosomal organelles (Figure 1g).³⁹ In contrast, inserting SP-B into the lipid coat also resulted in diffuse staining of the cytoplasm with Cy5-labeled siRNA (Figure 1h). In addition, the impact of SP-B on the intracellular distribution of NG-encapsulated single-stranded oligonucleotides (ONs) was investigated, using the same core–shell formulation (Figure 1e and f). Improved cytosolic delivery of ONs typically leads to its nuclear accumulation as previously reported in the literature.^{40–42} This effect was visualized for Alexa Fluor 647-labeled ONs only when the nanocomposite's lipid coat was supplemented with SP-B (Figure 1j), while the ONNG-LIP formulation typically led to its accumulation in the endolysosomes (Figure 1i).

Comparing Full-Length SP-B with the SP-B Mimicking Peptide KL4. Several peptide analogues of SP-B have been synthesized for surfactant replacement therapy. Among these, the KL4 peptide, with a sequence pattern inspired by the C-terminal end of SP-B and its cationic amphipathic character, was shown to reduce surface tension *in vitro* and *in vivo*.^{43–47} Besides these applications, the repurposing of KL4 for intracellular delivery of RNA therapeutics was demonstrated by Qiu and colleagues.^{38,48} Given the above, we replaced the molar fraction of SP-B (0.4 wt % = 0.04 mol %) in the siNG-LIP formulation with KL4 to assess its effect on siRNA delivery. However, in stark contrast to SP-B, the KL4 peptide was not able to improve the siRNA delivery efficiency of our formulation (Figure 2). These results suggest that the SP-B-

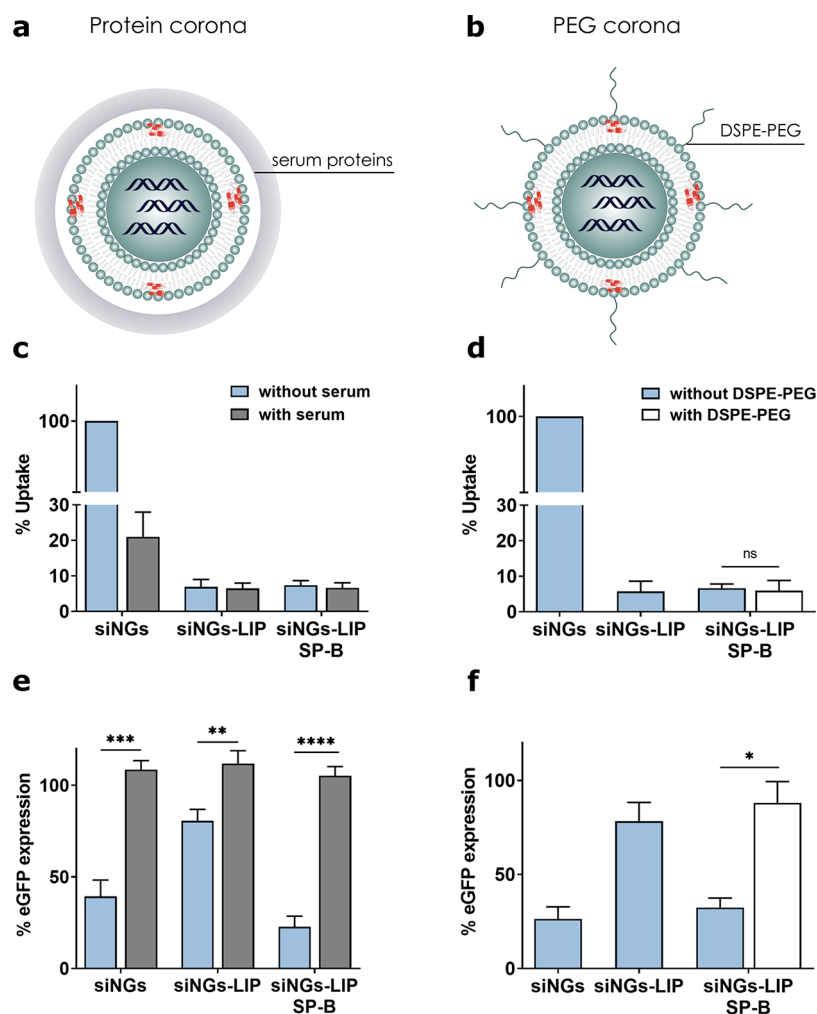


Figure 3. Impact of a hydrophilic protein or PEG corona on SP-B-mediated siRNA delivery. (a, b) Visual representations of the siNGs-LIP SP-B with a protein and stable PEG corona. (c) Flow cytometric quantification of siCy5 cellular uptake and (e) gene silencing of (un)coated formulations incubated in Opti-MEM (without serum, blue bars) and in cell culture medium (with serum, gray bars). (d) Flow cytometric quantification of siCy5 cellular uptake and (f) gene knockdown of siNGs and siNGs-LIP compared to siNGs-LIP SP-B with (white bars) and without 10 wt % DSPE-PEG₂₀₀₀. Data are represented as mean \pm SD of three independent repeats (statistical analysis was performed using multiple *t* tests; ns $p > 0.05$, ** $p \leq 0.01$, *** $p \leq 0.001$, **** $p \leq 0.0001$).

promoted siRNA delivery is not merely linked to its cationic amphiphilic nature, but that specific structural features and/or a specific orientation in membranes with defined lipid composition are likely required.

The Presence of a Protein or Poly(ethylene glycol) Corona Inhibits the Activity of SP-B. Independent of the possible nature of the induced membrane perturbation occurring between cellular membranes and the proteolipid bilayer of siNGs-LIP SP-B, direct contact between opposing membranes would be required.^{49,50} To indirectly probe the importance of membrane binding, we evaluated the impact of a hydrophilic corona, composed of serum proteins or poly(ethylene glycol) (PEG), on SP-B-promoted intracellular siRNA delivery. In the former case, the deposition of a protein corona was achieved *via* incubation of the siNG-LIP particles in a culture medium containing 10% fetal bovine serum (Figure 3a, c, and e). Of note, the presence of such a corona drastically lowered the intracellular uptake of the uncoated siNGs, possibly due to the shielding of the overall positive charge, impeding electrostatic interaction with the anionic cell membrane and/or *via* displacement of Cy5-labeled siRNA

from the nanogel surface.⁵¹ Contrarily, while the cellular uptake of the anionic siNGs-LIP (with and without SP-B) was not further reduced, the beneficial effect of SP-B on siRNA delivery and target gene silencing was completely nullified in the presence of serum. Second, we evaluated the impact of a hydrophilic polymer stealth layer, obtained by replacing 10 wt % of the DOPC phospholipid in the lipid coat with DSPE-PEG₂₀₀₀ (Figure 3b, d, and f). The successful PEGylation of the particles was reflected by the neutralization of the zeta potential (Supporting Figure 2). Similar to the protein corona, although the outer PEG layer did not further prevent endocytic uptake of siNGs-LIP, it completely blocked SP-B-mediated intracellular siRNA delivery. On the other hand, making use of a reversible PEGylation approach by replacing DSPE-PEG₂₀₀₀ with C8-PEG₂₀₀₀ ceramide did not negatively impact gene knockdown promoted by SP-B in Opti-MEM (Supporting Figure 3). As such sheathing coronas will create steric hindrance for SP-B, these data overall suggest that the SP-B protein in the outer lipid layer of the nanocomposites should be able to make close contact with (intra)cellular membranes to promote cytosolic siRNA delivery.

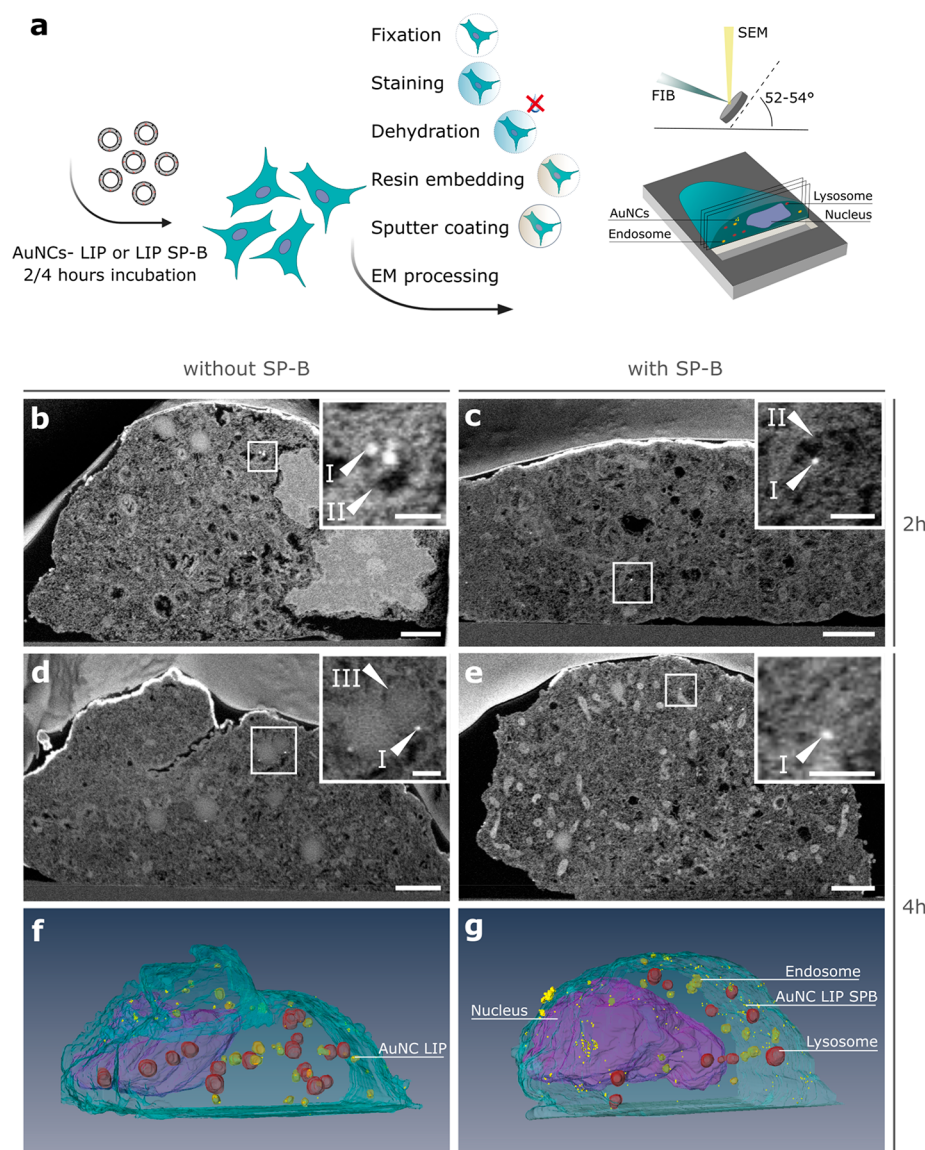


Figure 4. FIB-SEM imaging of the intracellular distribution of DOPC:PG (85:15 wt %) (LIP) liposomes with membrane-embedded gold nanoclusters (AuNCs) in H1299_eGFP cells. (a) Schematic illustration of FIB-SEM sample preparation and imaging. (b–e) Representative images of cell sections with close-ups in the insets showing regions of interest with the particles (I), endosomal membranes (II), and lysosomal membranes (III) indicated. (b) Two hour post-treatment of LIP:AuNC (– SP-B) liposomes and (c) 2 h post-treatment of LIP:AuNC (+ SP-B) liposomes showing both AuNC uptake inside endosomes. (d) Four hour post-treatment of LIP:AuNC (– SP-B) liposomes showing accumulation in lysosomes. (e) Four hour post-treatment of LIP:AuNC (+ SP-B) showing cytosolic presence and lack of presence in lysosomes. Scale bars = 2 μm in the main images and 500 nm in the insets. (f, g) Three-dimensional reconstructions of the cells shown in d and e, respectively.

Intracellular Distribution Studies of SP-B-Containing Liposomes via FIB-SEM. Having established that SP-B promotes cytosolic delivery of small nucleic acids and therefore likely requires direct membrane contact, we next performed focused ion beam scanning electron microscopy (FIB-SEM) measurements to assess differences in intracellular trafficking as a function of the presence of SP-B. Electron microscopy techniques are widely used to image the intracellular distribution of nanoparticles with high spatial resolution.⁵² Compared to transmission electron microscopy, FIB-SEM allows obtaining a 3D reconstruction of a cell by *in situ* serial sectioning and imaging, resulting in visualization of the spatial distribution of internalized NPs.^{52–54} For these experiments, we envisioned a simplified liposome model, composed of DOPC:PG (85:15 wt %) (LIP) with or without 0.4 wt % SP-B,

in line with previous experiments. To allow the intracellular visualization of the liposomes by SEM, lipophilic gold nanoclusters (AuNCs) (0.4 mg/2.5 mg lipids) were embedded in the lipid bilayer.⁵⁴ H1299_eGFP cells were incubated with the liposomes for 2 or 4 h and then fixed and prepared for imaging (Figure 4a). As shown in Figure 4b and c, after 2 h, LIP:AuNC liposomes both with and without SP-B induced endocytosis events at the level of the plasma membrane and accumulated inside endosomes (additional FIB-SEM slices are displayed in Supporting Figures 4 and 5, respectively). Of note, after 4 h of incubation, LIP:AuNC liposomes showed clear lysosomal and endosomal sequestration (Figure 4d and Supporting Figure 6), while the addition of SP-B rather elicited a cytosolic distribution of the AuNCs (Figure 4e and Supporting Figure 7), possibly due to endosomal escape events

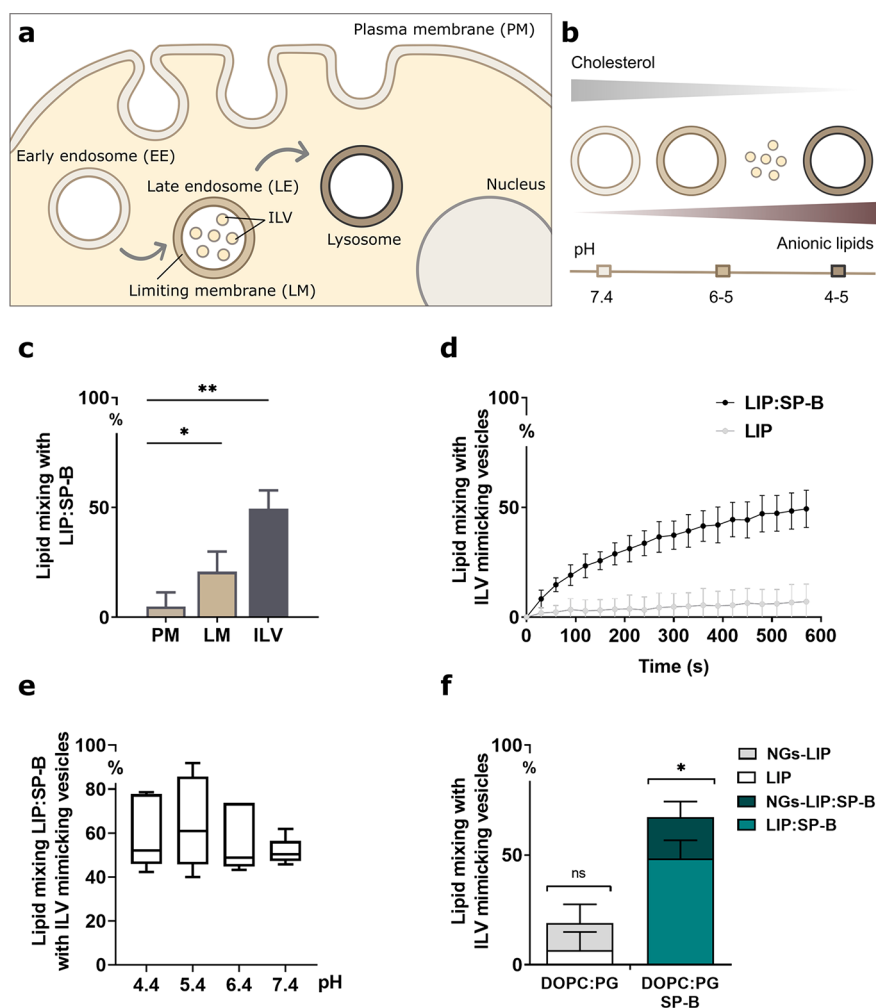


Figure 5. Lipid mixing of SP-B-containing liposomes and lipid-coated nanogels with liposome models of cellular membranes. (a, b) Changes in lipid composition and pH of cellular membranes and organelles. Plasma membrane (PM) and early endosomes (EE) mimicking liposomes were prepared using a molar ratio of PC:PE:Chol (55:15:30), pH 7.4. Limiting membranes of late endosomes (LM) were composed of PC:PE (96:4 mol %), while intraluminal vesicles (ILVs) were prepared using PG:PC:PE (77:19:4 mol %), both at pH 5.4. All the liposomes were prepared including 5.7 mol % of octadecyl rhodamine B chloride (R18) to allow the quantification of lipid mixing *via* dequenching kinetics. (c) Lipid mixing efficiency of DOPC:PG:SP-B (85:15:0.4 wt %) liposomes (LIP:SP-B) with different membrane models, measured after 10 min. (d) R18 dequenching kinetics of ILV with LIP or LIP:SP-B. Evaluation of (e) pH impact on lipid mixing between LIP SP-B liposomes and ILV-mimicking liposomes, measured after 10 min. (f) Lipid mixing efficiency of LIP or LIP-coated nanogels (NGs-LIP), with or without SP-B, measured after 10 min. An unpaired *t* test was used for statistical analysis for the latter (f), while one-way ANOVA was used for the others. Data are represented as mean \pm SD of three independent repeats, except for the pH assay ($n = 5$) (ns $p > 0.05$, * $p \leq 0.05$, ** $p \leq 0.01$, *** $p \leq 0.001$, **** $p \leq 0.0001$).

occurring between the two time points analyzed. A qualitative representation of the spatial AuNC-labeled liposome cytosolic distribution was obtained by 3D reconstruction of a cell incubated for 4 h with LIP:AuNC liposomes, with or without 0.4 wt % of SP-B (Figure 4f and g and Supporting Movies). In recent related work using the same AuNCs, the intracellular presence of AuNCs using a FIB-SEM lift-out procedure and subsequent STEM-EDX analysis was confirmed.⁵⁴ The high accelerating voltage needed to excite the $\text{La}1$ shell of gold would render *in situ* FIB-SEM EDX analysis not reliable due to the large resulting X-ray generation volume and the small amount of gold. Altogether, the presence of SP-B entails a markedly distinct intracellular distribution of the AuNC-labeled liposomes, while the absence of SP-B results in endosomal retainment and trafficking to lysosomes.

SP-B Induces Lipid Mixing with Anionic Endosomal Membranes. Different membrane-perturbing effects have

been described for SP-B, including the bridging of lipid membranes, membrane lysis, and membrane fusion, as well as lipid transfer and membrane remodeling.^{50,55,56} As membrane fusogenic activity has been described for SP-B within pulmonary surfactant and with bacterial membranes,^{27,50} we hypothesized that SP-B included in the siNG-LIP nanocomposites likewise orchestrates binding to and fusion with cellular membranes, leading to cytosolic siRNA delivery. To test this hypothesis, we first aimed to evaluate SP-B-promoted lipid mixing in vesicles with a composition mimicking that of the plasma membrane (PM), that of the limiting membrane (LM) of early/late endosomes (EE/LE), and that of intraluminal vesicles (ILVs) typically found in the lumen of late endosomal multivesicular bodies (MVBs) (Figure 5a and b). These simplified vesicular membrane models were prepared including self-quenching concentrations of octadecyl rhodamine B chloride (R18) to enable quantification of the

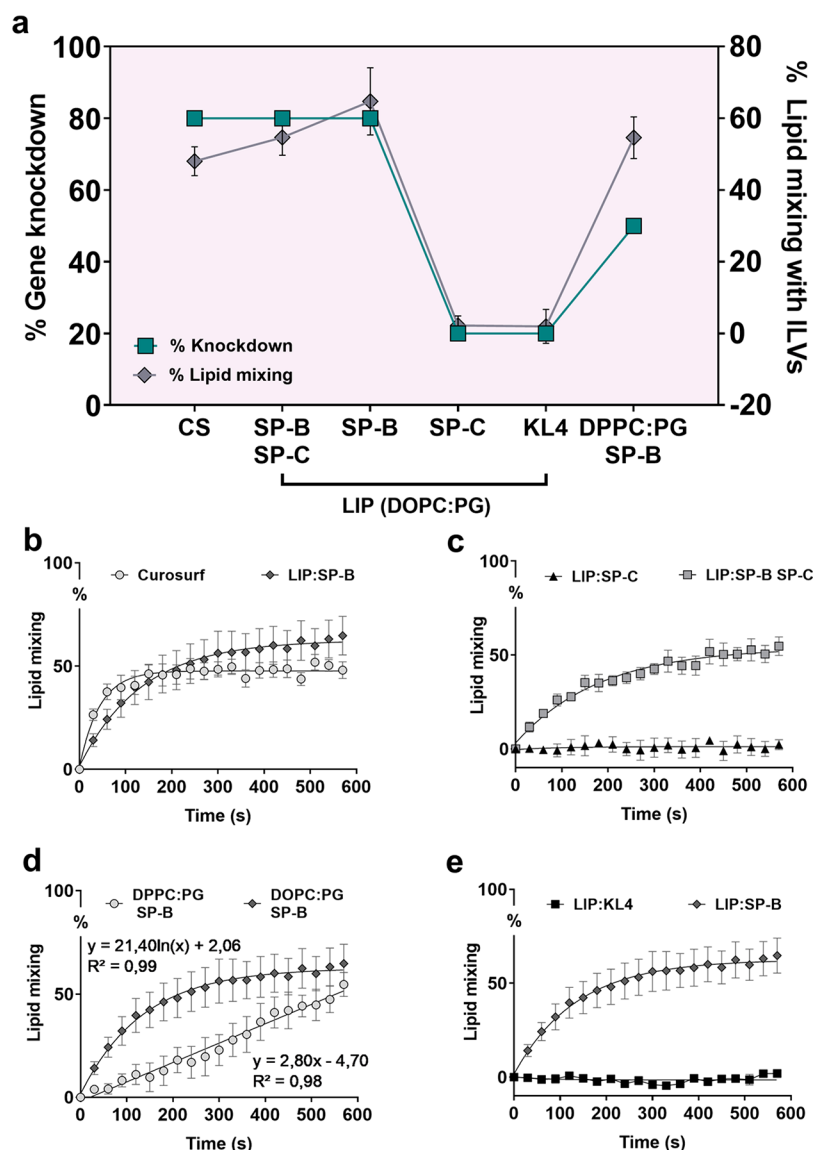


Figure 6. Correlation of lipid mixing with intracellular siRNA delivery. (a) Correlation between extent of knockdown efficiency (siRNA-mediated eGFP silencing in H1299 eGFP cells) and lipid mixing. Gene silencing percentages of Curosurf (CS), SP-C, SP-B:SP-C, and DPPC:SP-B were taken from Merckx *et al.* and Guagliardo *et al.*^{19,20} The extent of lipid mixing was measured with ILV-mimicking vesicles (PG:PC:PE, 77:19:4 mol %) for all panels of the figure. (b) Lipid mixing of the porcine surfactant formulation CS compared to DOPC:PG (LIP)-SP-B (data are shown as a mean \pm SEM of a technical triplicate for CS). (c) Lipid mixing of LIP:SP-C compared to LIP:SP-B SP-C (0.4 wt % SP-B; 0.7 wt % SP-C) (data are shown as a mean \pm SEM of two independent repeats). (d) ILV lipid mixing of DOPC:PG:SP-B compared to DPPC:PG:SP-B (data are shown as a mean \pm SEM of three independent repeats). (e) Lipid mixing of LIP:SP-B compared to LIP:KL4 (data are shown as a mean \pm SEM of a technical triplicate).

lipid mixing efficiency by following the kinetics of R18 dequenching.^{57–59} This process follows the dilution of the probe into the larger surface of merged membranes, in this case occurring upon fusion with unlabeled liposomes or lipid-coated NGs. For the PM (as well as EE), a lipid composition of PC:PE:Chol (55:15:30 mol %) was selected to simulate the concentration of cholesterol, critical to form a fluid phase (involved in endocytosis, protein mobility, and lipid diffusion). For the LE compartment, next to probing the influence of acidic pH, we aimed to discriminate the impact of anionic lipids, working with LM-like vesicles made of the zwitterionic mixture PC:PE (96:4 mol %). ILVs were mimicked by vesicles composed of anionic PG:PC:PE (77:19:4 mol %) (Figure 5b).⁶⁰ As shown in Figure 5c, SP-B induced only lipid mixing of DOPC:PG (85:15 wt %) liposomes with vesicles mimicking

the LE compartment, with fusion being most pronounced with the anionic ILV-like vesicles. No fusion was observed with any of the tested vesicles in the absence of SP-B (Figure 5d). Of note, while previous reports have used SP-B protein concentrations in the range of 0.2–1 mol %, corresponding to 2–10 wt % in a rigid DPPC:PG lipid mixture, here we investigated lipid mixing with 0.4 wt % of SP-B in the more fluid DOPC:PG lipid composition.⁶¹ *In cellulo*, ILV membranes are highly enriched with the fusogenic bis-(monoacylglycerol)phosphate (BMP), an anionic lipid species specific to late endosomes and lysosomes.⁶² Fusion kinetics of SP-B-containing vesicles with an ILV model membrane containing BMP as main anionic species (Supporting Figure 8a) show a similar trend to the one reported in Figure 5d. On the other hand, pretreatment of the cells with a BMP-binding

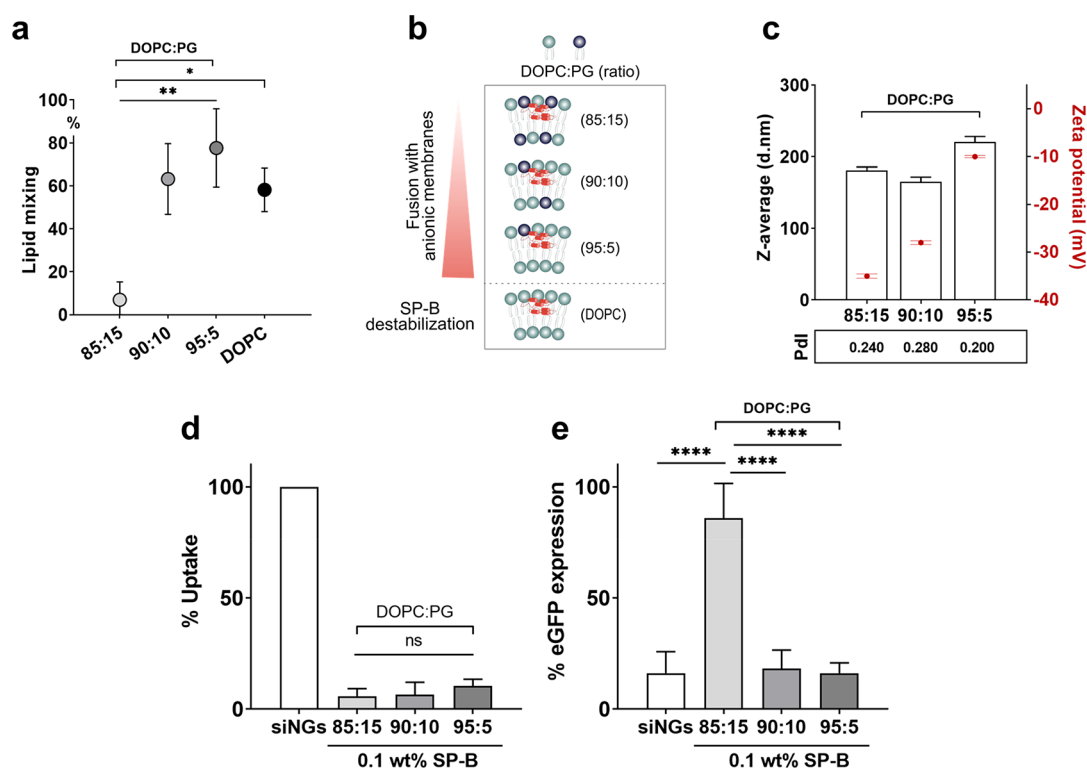


Figure 7. Impact of negatively charged phospholipid concentration in the proteolipid coating on siNGs-LIP SP-B biological activity. (a) Lipid mixing with ILV-mimicking vesicles of DOPC:PG (different ratios) liposomes, supplemented with 0.1 wt % of SP-B. (b) Schematic illustration of the increased lipid mixing of SP-B-containing liposomes related to the decreased amount of anionic lipids. (c) Hydrodynamic diameter (nm), polydispersity index (PDI), and zeta potential of the DOPC:PG liposomes with differing amounts of PG. (d) Cellular uptake and (e) gene silencing potential of siNGs layered with different DOPC:PG ratios (85:15, 90:10, 95:5 wt %) in the presence of 0.1 wt % of SP-B. Data are shown as mean \pm SD of three independent repeats (statistical analysis was performed using one-way ANOVA; ns $p > 0.05$, * $p \leq 0.05$, ** $p \leq 0.01$, *** $p \leq 0.001$, **** $p \leq 0.0001$).

antibody did not block target gene knockdown, altogether suggesting the dominant importance of negative charge in SP-B membrane binding and fusion, rather than a specific interaction with the BMP lipid (Supporting Figure 8b). As the intraendosomal pH markedly acidifies upon endosomal maturation, we additionally assessed the extent of SP-B-promoted lipid mixing with ILV-mimicking vesicles at varying pH. As illustrated in Figure 5e, lipid mixing occurred in all tested conditions, ranging from lysosomal (pH 4.4) to extracellular (pH 7.4) pH. Treating the cells with bafilomycin, a macrolide inhibitor of the vacuolar proton pump known to block endosomal acidification, did not impede SP-B-promoted gene knockdown, thus endorsing the pH independence of SP-B activity (Supporting Figure 9). Finally, since the SP-B LIP in the performed gene silencing experiments is supported by a siRNA-loaded cationic dextran NG core, we next quantified R18 dequenching with DOPC:PG (85:15 wt %)-coated NGs as well. Interestingly, as shown in Figure 5f, the presence of the NG core promotes SP-B-dependent lipid mixing with anionic membranes, although the underlying mechanism remains obscure.

Correlation of SP-B-Mediated Fusion with siRNA Delivery. The aforementioned fusion experiments were performed with vesicles bearing a DOPC:PG:SP-B (85:15:0.4 wt %) lipid composition, for which SP-B-promoted gene silencing was demonstrated in earlier work and confirmed in Figure 1 to be related to improved cytosolic siRNA delivery. To further validate the correlation of SP-B-induced membrane binding and fusion with the enhanced cytosolic delivery of

siRNA, we next examined the fusogenicity of different proteolipid mixtures with their relative gene silencing efficiency. An overview of the different proteolipid mixtures and the correlation between knockdown efficiency and lipid mixing is illustrated in Figure 6a. As mentioned in the introduction, the initial observation that PS could be repurposed as RNA delivery enhancing biomaterial was based on the clinical surfactant formulation Curosurf, which contains both hydrophobic surfactant proteins (SP-B and SP-C). Here, we could show that also Curosurf-derived liposomes promoted lipid fusion under equal experimental conditions (Figure 6b). We previously reported that the positive effect of SP-B on siRNA delivery could not be replicated by its partner hydrophobic surfactant protein SP-C, which is likewise involved in lung surfactant stabilization.¹⁹ This absence of cytosolic siRNA delivery correlates with a lack of ILV membrane fusion with SP-C proteolipid vesicles (Figure 6c). In line with this finding, it was additionally demonstrated that SP-C does not block either the fusogenic activity of SP-B in a DOPC:PG (85:15 wt %) bilayer nor the siRNA-mediated gene silencing for this protein combination, as reported earlier.¹⁹ Additionally, we confirmed the inability of the synthetic C-terminal mimic KL4 to induce lipid mixing (Figure 6e), which correlates with the previously shown lack of intracellular siRNA delivery (Figure 2b). As both SP-C and KL4 display cationic amphiphilic properties, these data suggest that mere electrostatic binding does not suffice to promote membrane fusion. Of note, both SP-C and KL4 show a deep transmembrane insertion in lipid bilayers, as opposed to the

peripheral location of SP-B in surfactant membranes.^{30,63} In addition, in contrast to SP-C and KL4, SP-B exists as a covalent dimer, a structural feature that is linked to SP-B's ability to bridge phospholipid membranes.⁶⁴ Such structural differences could in part explain differences in fusogenic behavior. Previous work by our group established a strong influence of the lipid composition on SP-B's activity, with reduced siRNA delivery efficiency when the fluid lipid DOPC was replaced by its rigid counterpart DPPC. Reflecting the outcome of the transfection experiments,^{19,20} although the final extent of fusion within the time frame tested is comparable, the insertion of SP-B into DPPC:PG (85:15 wt %) bilayers consistently demonstrated much slower lipid mixing kinetics with ILV model membranes (Figure 6d). A possible explanation for this discrepancy could involve the impact of phospholipid saturation and membrane fluidity in the lateral distribution of the protein that may be required to assemble the higher order supradimeric ring-like SP-B oligomers. The latter has been described to mediate intermembrane connection and lipid transfer activity and/or further protein clustering into highly fusogenic domains.⁶⁵ Altogether, these data demonstrate a strong positive correlation between the fusogenic activity of SP-B and its capacity to promote cytosolic siRNA delivery.

Promoting SP-B-Induced Membrane Fusion by Reducing Electrostatic Repulsion. As shown in Figure 5e, neutralization of pH does not interfere with SP-B's fusogenic effect, hinting toward its reliance on the presence of negatively charged lipids in the opposing membrane instead of pH-induced changes in its charge density or conformation. The results obtained so far indicate that upon endocytosis of SP-B-supplemented lipid-coated nanogels, the positively charged SP-B would preferentially interact with anionic domains found in ILVs or the late endosomal LM. As it was previously found that the membrane-perturbing effect of anionic SP-B proteolipid vesicles on negatively charged bacterial membranes was hampered by electrostatic repulsion,⁶⁶ we hypothesized that a reduction of the anionic PG fraction in the SP-B proteolipid coat of the nanocomposites could facilitate its interaction with the anionic LE membranes. To evaluate this, we assessed the effect of reduced PG content (DOPC:PG 85:15; 90:10; 95:5 wt % and only DOPC) on lipid mixing and siRNA delivery. To better observe lipid composition-induced differences, we likewise lowered the SP-B fraction to 0.1 wt % of the total lipid amount. As shown in Figure 7a and b and in support of our hypothesis, lowering the PG percentage in SP-B liposomes strongly increased its fusogenic effect with anionic ILVs, although a minimal fraction of anionic species seems required, as previously reported.^{67,68} As expected, coating siNGs with these different proteolipid mixtures resulted in comparable size but decreased anionic charge as a function of PG reduction (Figure 7c). Most importantly, despite equivalent intracellular siRNA doses (Figure 7d), the less negatively charged proteolipid coatings reached 80% knockdown (Figure 7e) with only 0.1 wt % of SP-B, clearly outperforming the initial DOPC:PG (85:15 wt %) composition for which knockdown was nearly absent. As the improved fusogenic activity was mirrored by a strongly promoted siRNA-mediated target gene knockdown, this observation further strengthens the correlation between electrostatic interaction, lipid fusion, and cytosolic siRNA delivery. Still, we cannot fully exclude that the enhanced intracellular delivery promoted by SP-B could in part also be

influenced by modulation of intracellular trafficking. For instance, it is known that endocytosis of SP-B-containing surfactant complexes in type II alveolar cells is followed by recycling to lamellar body compartments, instead of accumulation in lysosomes.⁶⁹ How such changes in intracellular processing would impact siRNA delivery and to what extent it would be cell type-dependent requires further exploration.

Toward a Model for SP-B-Promoted Cytosolic siRNA Delivery. As demonstrated above, membrane fusion appeared to be highly dependent on the presence of negatively charged lipids such as PG in the opposing membrane. The reliance on anionic lipids is in line with many literature reports stating the importance of the (electrostatic) interaction of PG with the positively charged SP-B toward its alveolar surfactant activity.⁶¹ This electrostatic interaction is conceivable given that SP-B exists as a covalent dimer with a net positive charge of +14. In addition, SP-B belongs to the saposin-like family of proteins (SAPLIP), of which several other members (*e.g.*, NK-lysin, granulysin) bear positively charged amino acids that mediate interaction with negatively charged membranes.^{50,66} Following endocytosis, nanocarriers are typically confined in early endosomes having a lipid membrane composition similar to the plasma membrane.^{70–72} From this initial sorting organelle, the endocytosed SP-B proteolipid-coated nanogels are routed to the late endosomal compartment, where the accessible SP-B molecules can electrostatically interact with anionic lipids, including BMP. The latter lipid is a structural isomer of PG, specific for the late endosomal/lysosomal compartment. While its presence in the luminal leaflet of the limiting membrane is scattered in anionic microdomains, it reaches high concentrations in the membranes of so-called ILVs. BMP is known to adopt an inverted conical shape by which it stimulates fusion.^{60,73} The markedly promoted membrane fusion upon interaction of SP-B-containing proteolipid mixtures with anionic vesicles (including BMP-enriched vesicles), instead of zwitterionic vesicles observed *in vitro*, also strongly indicates that upon endocytic uptake SP-B could mediate membrane fusion *via* interaction with late endosomal (BMP-enriched) membranes. In support of this hypothesis, such fusion events have also been convincingly demonstrated for several viruses (*e.g.*, dengue virus, vesicular stomatitis virus, phleboviruses) and cell-penetrating peptides (*e.g.*, HIV-derived TAT) to promote endosomal escape and cytosolic delivery of macromolecules.^{74–78} On the basis of the above, we propose a cytosolic siRNA delivery model for SP-B proteolipid-coated NGs as schematically presented in Figure 8. According to this model, following endocytic uptake and subsequent trafficking toward the late endosomal compartment, the cationic SP-B would promote the endosomal escape of siRNA either (1) directly, *via* fusion with anionic microdomains present in the LM, or (2) indirectly, *via* “back-fusion” promoted by ILVs, an endogenous process occurring in LE.^{78–81} Interestingly, in contrast to such viral proteins and peptides, SP-B-mediated fusion was proven independent of both the specific structure of the BMP lipid and acidic endosomal pH, the latter validating earlier reports in the literature.^{50,66} As such, it cannot be excluded that SP-B likewise initiates fusion events in other cellular compartments, provided that anionic lipids are exposed for SP-B engagement.

CONCLUSIONS

Therapeutic application of RNA drugs is limited by the need for delivery systems that allow efficient cytosolic release. The

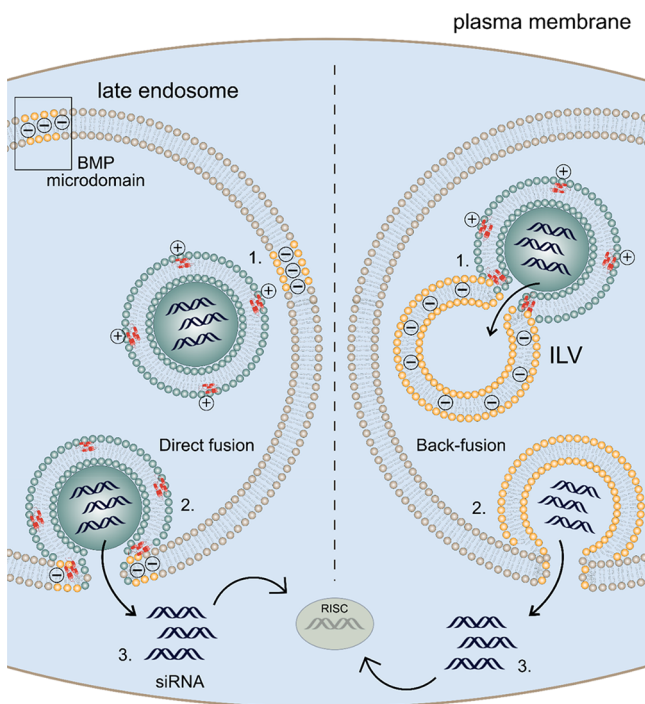


Figure 8. Proposed model for mode-of-action of SP-B-mediated siRNA delivery. SP-B proteolipid coated NGs are internalized *via* endocytosis, for which the internalization efficiency is independent from the presence of SP-B in the outer layer. Once endocytosed, the NPs are trafficked toward the late endosomal compartment, enriched in negatively charged endogenous lipids (BMP, phosphatidylserine, and phosphatidylinositol). These lipids can be present in limiting membrane microdomains (illustrated in the figure upper left) or in so-called intraluminal vesicles (ILVs). Similar to fusion events described for a selection of viral envelopes or cell-penetrating peptides, the interaction of the SP-B proteolipid shell with these anionic endosomal membranes would allow the cytosolic release of the encapsulated siRNA, either directly (*via* fusion with the LM, illustrated on the left) or indirectly (*via* fusion with ILVs, followed by back-fusion with the limiting membrane, illustrated on the right). The siRNA released in the cytosol is consequently available to interact with the RNA-induced silencing complex (RISC).

cationic amphiphilic lung surfactant protein B (SP-B) plays an essential role in lung surfactant dynamics and mammalian breathing.^{23,30,82,83} It has been widely reported that SP-B contributes to pulmonary surfactant storage and secretion by alveolar type II epithelial cells as well as its stabilization and recycling at the alveolar air–liquid interface. Although great progress has been made in unraveling the biophysical role of SP-B in lung surfactant activity, the 3D conformation of the SP-B protein and its detailed molecular mechanism have not yet been defined.⁸⁴ In addition to the well-known function of SP-B at the alveolar spaces, we recently discovered a previously unknown property of SP-B in its ability to promote siRNA-mediated gene knockdown, suggesting that this highly specialized protein can also interfere with (intra)cellular membranes.^{16,17,19,20} In this work, it was demonstrated that SP-B can promote cytosolic siRNA delivery *via* electrostatic interaction and subsequent fusion with anionic lipid membranes, typically found in late endosomal compartments. In contrast to using viral-derived peptides or membrane-perturbing toxins, repurposing an endogenous membrane-active protein such as SP-B as an siRNA delivery-promoting

agent offers the opportunity to achieve safe and efficient siRNA delivery, in particular for local administration such as inhalation therapy. We anticipate that the gained mechanistic insights into how SP-B can mediate cytosolic siRNA delivery will fuel the rational design of the next generation of SP-B-inspired nanocarriers for improved intracellular siRNA delivery.

EXPERIMENTAL SECTION

Small Interfering RNAs and Single-Stranded Oligonucleotides. Twenty-one-nucleotide siRNA duplexes were purchased from Eurogentec (Seraing, Belgium). The sequences used are listed as follows. For siRNA targeting enhanced green fluorescent protein (siEGFP): sense strand = 5'-CAAGCUGACCCUGAAGUUCt-3'; antisense strand = 5'-GAACUUCAGGGUCAGCUUGt-3'. For nontargeting negative control sequence (siCTRL): sense strand = 5'-UGCGCUACGAUCGACGAUGt-3'; antisense strand = 5'-CAUCGUCGAUCGUAGCGCAtt-3'. The concentration of the siRNA solutions in nuclease-free water (Ambion-Life Technologies, Ghent, Belgium) was calculated *via* absorption measurements at 260 nm (1 OD₂₆₀ = 40 μg/mL) with a NanoDrop 2000c UV–vis spectrophotometer (Waltham, MA, USA). Fluorescently labeled siRNA was obtained through modification of siCTRL with a Cy5 dye at the 5' end of the sense strand (siCy5). For AF647-oligonucleotides (ONs) = 5'-gaacttcagggtcagcttgg-3'. Alexa Fluor 647 labeled (5' end) 21-mer ONs were obtained from Eurogentec (Seraing, Belgium). Capital and lower case letters represent ribonucleotides and 2'-deoxyribonucleotides, respectively.

Synthesis of Dextran Nanogels and siRNA Complexation. Using an inverse miniemulsion photopolymerization method as previously reported,^{85–88} dextran hydroxyethyl methacrylate (dex-HEMA, degree of substitution (DS) of 5.2) was copolymerized with a cationic methacrylate monomer (2-(methacryloyloxy)ethyl trimethylammonium chloride (TMAEMA)) to form cationic dex-HEMA-co-TMAEMA nanogels (dex-HEMA NGs).^{17,19} The obtained nanogels (NGs) were lyophilized and stored desiccated to ensure long-term stability. To produce siRNA-loaded nanogels (siNGs) or ON-loaded nanogels (ONNGs), equal volumes of siRNA/ON and NGs in (4-(2-hydroxyethyl)-1-piperazineethanesulfonic acid) (HEPES) buffer (20 mM, pH 7.4) were mixed and allowed to incubate for ≥10 min on ice.

Lipids, Surfactant Protein B, and KL4. To prepare liposomes and proteolipid-coated NGs, the following lipids were purchased from Avanti Polar Lipids (Alabaster, AL, USA) in chloroform: 1,2-dioleoyl-*sn*-glycero-3-phosphocholine (DOPC), 1- α -phosphatidylglycerol from egg yolk (eggPG), *N*-octanoyl-sphingosine-1-{succinyl[methoxy-(polyethylene glycol)₂₀₀₀]} (C8 PEG₂₀₀₀ Ceramide), 1,2-dipalmitoyl-*sn*-glycero-3-phosphocholine (DPPC), 1,2-distearoyl-*sn*-glycero-3-phosphoethanolamine-*N*-[methoxy-(polyethylene-glycol)₂₀₀₀] (DSPE-PEG₂₀₀₀), cholesterol (Chol), 1-palmitoyl-2-oleoyl-*sn*-glycero-3-phosphoethanolamine (POPE), *sn*-(3-oleoyl-2-hydroxy)-glycerol-1-phospho-*sn*-1'-(3'-oleoyl-2'-hydroxy)-glycerol (ammonium salt) (BMP). Octadecyl rhodamine B chloride was purchased from Thermo Fisher Scientific (Aalst, Belgium) and dissolved in DMSO. SP-B was extracted and purified from native porcine pulmonary surfactant following a procedure described earlier by Pérez-Gil and co-workers.²⁷ A stock of the protein in chloroform/methanol (2:1, v/v) was used for the experiments. KL4 peptide with the sequence KLLLLLLLLL-KLLLLLLLLL was synthesized in the laboratory of Prof. David Andreu (Pompeu Fabra University, Barcelona, Spain).

Preparation of Proteolipid-Coated Nanogels. The lipids with or without SP-B (0.4 wt %, unless specified otherwise) were mixed in chloroform at the required weight ratios (described for each experiment), and a (proteolipid) film was obtained *via* nitrogen flow or rotary evaporation. The lipid film was then hydrated using HEPES buffer (20 mM, pH 7.4) and subsequently mixed with equal volumes of the siNGs (15 mg lipid/mg nanogel, as previously optimized).^{15,19} Following a ≥10 min incubation on ice and three 10 s cycles of high-energy sonication (amplitude 10%), using a probe sonicator (Branson Ultrasonics Digital Sonifier, Danbury, CT, USA),

(proteo)lipid-coated siNGs (siNGs-LIP/siNGs-LIP SP-B) were obtained. Hydrodynamic diameter, PDI, and zeta potential of all formulations were measured *via* dynamic light scattering (Zetasizer Nano, Malvern Instruments, Worcestershire, UK).

Lipid Mixing Assay. To obtain R18-labeled vesicles that mimic (intra)cellular membranes, lipids and R18 (5.7 mol %) were mixed in chloroform/methanol (2:1 v/v) in the indicated ratios, and a lipid film was obtained *via* rotary evaporation. The following lipid compositions (mol %) were selected: for the plasma membrane (PM) and early endosomes (EE) PC:PE:Chol (55:15:30), for the limiting membrane (LM) of late endosomes PC:PE (96:4), and for intraluminal vesicles (ILVs) of late endosomes PG:PC:PE (77:19:4), as previously reported in the literature.⁶⁰ Lipid films were hydrated using a tris-maleate buffer (50 mM) with pH 7.4 for PM-mimicking liposomes or pH 5.4 for LM and ILVs. Lipid dispersions were then sonicated for 1 min (10% amplitude) using a probe sonicator (Branson Ultrasonics Digital Sonifier, Danbury, CT, USA). The R18-containing vesicles were diluted to a final lipid concentration of 1.25 μM before mixing with SP-B-containing liposomes or lipid-coated nanogels. For the lipid mixing assay, siNGs-LIP/siNGs-LIP SP-B or LIP/LIP SP-B were prepared at a final lipid concentration of 5 mg/mL. To follow lipid mixing kinetics, 200 μL of R18 vesicles was mixed with 10 μL of SP-B-containing liposomes or lipid-coated NGs in a 96-well plate (Greiner Bio-One GmbH, Kremsmünster, Austria). R18 vesicles disrupted with 1 wt % Triton X-100 were used as a positive control. All fluorescence measurements were performed using a Wallac Envision multilabel reader (PerkinElmer, Zaventem, Belgium). The percentage of lipid mixing was calculated at different time points based on the following equation:

$$\% \text{lipid mixing} = [(I_x - I_0)/(I_{100} - I_0)] \times 100$$

where I_x represents the R18 fluorescence intensity measured at time x , I_0 the R18 fluorescence intensity measured at time 0, and I_{100} the fluorescence after the addition of Triton X-100.

Cell Line and Culture Conditions. Cell culture experiments were performed using a human non-small-cell lung cancer cell line stably expressing eGFP (H1299_eGFP), kindly provided by the lab of Prof. Camilla Foged (Department of Pharmacy, University of Copenhagen, Copenhagen, Denmark).^{19,20} H1299_eGFP cells were cultured in a cell culture medium (CCM) composed of RPMI 1640, supplemented with 2 mM glutamine, 100 U/mL penicillin/streptomycin, and 10% (v/v) fetal bovine serum. Cells were cultured at 37 °C in a humidified atmosphere containing 5% CO₂ and were passed every 3 days using a 0.25% (w/v) trypsin/ethylenediaminetetraacetic acid solution to maintain subconfluency. All cell culture materials were purchased from Gibco-Life Technologies, except for the serum, which was obtained from Hyclone (Thermo Fisher Scientific, Waltham, MA, USA).

Quantification of Cellular Uptake of siRNA *via* Flow Cytometry. To quantify the cellular internalization of siRNA *via* flow cytometry, H1299_eGFP cells (2×10^4 cells/cm²) were seeded in 24-well or 96-well plates (Greiner Bio-One GmbH, Kremsmünster, Austria) and allowed to settle overnight. NGs complexing a mixture of siCTRL and siCy5 were coated with a (proteo)lipid mixture using the procedure described above. After complexation, the particles were diluted 1:5 in Opti-MEM to obtain a final NG concentration of 30 $\mu\text{g}/\text{mL}$ and incubated with the cells for 4 h (37 °C, 5% CO₂). Next, to remove cell-surface-bound fluorescence, the cells were washed with dextran sulfate sodium salt (0.1 mg/mL in PBS) before flow cytometric quantification, using the CytoFLEX flow cytometer (Beckman Coulter, Krefeld, Germany) and CytExpert software. Data analysis was performed using FlowJo (version 10.5.3, Treestar, Costa Mesa, CA, USA). The mean fluorescence intensity (MFI) of the coated siNG formulations was normalized to the uncoated ones. To probe the influence of SP-B on the intracellular persistence of siRNA, transfected cells were fixed with paraformaldehyde (4% in PBS) for 15 min at room temperature at different time points post-transfection (*i.e.*, 4 + 0 h, 4 + 1 h, 4 + 2 h, 4 + 4 h, and 4 + 24 h). Flow cytometric quantification and data analysis were performed as

described above. Here, the MFI of transfected cells was normalized to the 4 + 0 h time point.

Effect of Endocytic Uptake Inhibitors on the Cellular Uptake of (Proteo)lipid-Coated Nanogels. H1299_eGFP cells (2×10^4 cells/cm²) were plated in 96-well plates (Greiner Bio-One GmbH, Kremsmünster, Austria) and allowed to settle overnight. NGs were loaded with 100 nM Cy5-labeled siRNA and coated with LIP or LIP:SP-B, as described above. After complexation, the particles were diluted 1:5 in Opti-MEM to obtain a final NG concentration of 30 $\mu\text{g}/\text{mL}$. First, the cells were preincubated for 30 min (37 °C, 5% CO₂) with mounting concentrations of the endocytic uptake inhibitors chlorpromazine, nystatin, and EIPA. Subsequently, the cells were co-incubated for 3 h (37 °C, 5% CO₂) with siNG-LIP or siNG-LIP SP-B and inhibitors. Next, the cells were washed with dextran sulfate sodium salt (0.1 mg/mL in PBS) to remove cell-surface-bound fluorescence before flow cytometric analysis. Only the conditions with an estimated $\geq 50\%$ remaining cells compared to nontreated control were included. The MFI of transfected cells was normalized to the condition without inhibitor.

Quantification of EGFP Gene Silencing *via* Flow Cytometry. To quantify gene knockdown efficiency, H1299_eGFP cells (2×10^4 cells/cm²) were plated in 24-well or 96-well plates (Greiner Bio-One GmbH, Kremsmünster, Austria) and allowed to settle overnight. Coated and uncoated siNG formulations were prepared in Opti-MEM and incubated with the cells (final siRNA concentration of 50 nM, unless stated otherwise) as described above. After a 4 h incubation, cells were washed with PBS and incubated with fresh CCM for 48 h. Next, cells were prepared for flow cytometry as described above. The percentage of eGFP expression was calculated by normalizing the MFI of cells treated with siEGFP to the MFI of cells treated with siCTRL. The samples were measured using the CytoFLEX flow cytometer (Beckman Coulter, Krefeld, Germany) and CytExpert software. Data analysis was performed using the FlowJo analysis software (version 10.5.3).

Visualization of siCy5 and AF647-ON Cytosolic Delivery *via* Confocal Microscopy. H1299_eGFP cells were seeded in 35 mm diameter glass-bottom microscopy dishes #1.5 (125 000 cells/dish) (Greiner Bio-One GmbH, Germany) and were allowed to settle overnight. To visualize the siCy5 and AF647-ON cytosolic delivery, NGs-LIP or NGs-LIP SP-B (30 $\mu\text{g}/\text{mL}$ NGs complexing 100 nM siCy5 or 50 nM AF647-ON) were added to the cells in Opti-MEM. After 4 h of incubation (37 °C, 5% CO₂), cells were washed with dextran sulfate sodium salt (0.1 mg/mL in PBS) and incubated with CCM for 1 h. Before imaging, nuclei were stained using Hoechst 33342 (Molecular Probes, Belgium) diluted 1/10000 in CCM. A spinning disk confocal microscope (Nikon Eclipse Ti, Japan), equipped with an MLC 400 B laser box (Agilent Technologies, CA, USA), a Yokogawa CSU-X confocal spinning disk device (Andor, Belfast, UK), an iXon Ultra EMCCD camera (Andor Technology, Belfast, UK), a Plan Apo VC 60 \times 1.4 NA oil immersion objective lens (Nikon, Japan), and NIS Elements software (Nikon, Japan) was used for imaging. The 408 and 633 nm laser lines were applied sequentially to excite the Hoechst-stained nuclei and the siCy5 or AF647-ON, respectively. To allow better detection of cytosolic/nuclear staining, a long exposure time of 500 ms was applied as previously reported for the 633 nm laser.³⁹ To visualize the Hoechst-stained nuclei using the 408 nm laser, an exposure time of 50 ms was maintained. The obtained images were analyzed using Fiji (ImageJ).

Preparation of AuNC Liposomes for Focused Ion Beam–Scanning Electron Microscopy. The lipids with or without SP-B (DOPC:eggPG 85:15 or DOPC:eggPG:SP-B 85:15:0.4 wt %) were mixed in chloroform, and a (proteo)lipid film was obtained *via* rotary evaporation. The lipid film was then hydrated using HEPES buffer (20 mM, pH 7.4). Gold nanoclusters (AuNCs) were synthesized as previously reported by Kauscher *et al.*⁵⁴ To allow the insertion of AuNCs, a solution of AuNCs in tetrahydrofuran (10 mg/mL) was added to the lipid dispersion to obtain a final lipid:AuNCs ratio of 1:0.18. The (proteo)lipid:AuNC dispersion was then vortexed 2 \times 30 s and subsequently sonicated for 30 s (amplitude 20%), using a probe sonicator (Sonics Vibra-cell, Newton, CT, USA). Purification of the

AuNC liposomes was performed using a qEV Izon Science Ltd. size exclusion chromatography column. The portion of AuNC liposomes, identified by their color, was collected. Adding 500 μL of AuNC liposome solution to the column, about 1 mL of the eluate was recovered, resulting in an approximately 2-fold dilution. AuNCs LIP/LIP SP-B were diluted in Opti-MEM and incubated with the cells (final lipid concentration of 0.240 mg/mL).

FIB-SEM Sample Preparation. FIB-SEM sample preparation was performed following a procedure as previously reported by Kauscher *et al.*⁵⁴ Chemicals were obtained from Electron Microscopy Sciences (USA) unless specified otherwise. In brief, H1299_eGFP cells were seeded at 25 000 cells/cm² in a 24-well plate on 10 mm glass coverslips (VWR, U.K.) sterilized in 70% (v/v) ethanol and washed twice with PBS (Gibco U.K.). The cells were allowed to adhere overnight, after which the cells on the coverslips were replated and incubated for 2 and 4 h with LIP or LIP SP-B liposomes containing AuNCs (preparation described in the previous section). At the assigned time point, the cells were washed with PBS and fixed for 15 min at 37 °C, 5% CO₂, in 4% (w/v) EM-grade and washed a further three times with PBS. Preparation for FIB-SEM was continued by washing the samples 2 \times 5 min in 0.1 M cacodylate buffer in dH₂O. Postfixing was performed for 1 h in 2.5% (w/v) EM-grade glutaraldehyde in 0.1 M cacodylate buffer. Samples were washed 2 \times 5 min in 0.1 M cacodylate buffer, stained for 1 h in 1% (w/v) OsO₄ in 0.1 M cacodylate buffer, and washed 2 \times 5 min in dH₂O. Additional staining steps were performed by incubation of the samples for 1 h in 1% (w/v) tannic acid and 2.5 h in uranyl acetate, both in dH₂O, and filtered through a 0.2 μm syringe filter, with 2 \times 5 min washes with dH₂O in between. Samples were serially dehydrated by 2 \times 5 min washes in an ethanol/water gradient of 20%, 30%, 50%, and 70% (v/v) ethanol. Samples were kept overnight in 70% (v/v) ethanol, after which dehydration was completed by 2 \times 5 min washes in 80% and 90% (v/v) ethanol and 4 \times 5 min washes in 100% ethanol. Resin embedding was performed by gradient infiltration with 3:1, 2:1, and 1:1 (v/v) ethanol and epoxy resin (epoxy embedding medium kit, Sigma-Aldrich, U.K.) for 2.5 h each and subsequently 1:2 overnight. Then the resin infiltration was completed by 2 \times 2.5 h incubation in full resin. The excess of resin was removed by ethanol spraying the samples and blotting to achieve minimal resin embedding. The resin was cured in an oven at 60 °C for 72 h, placing the coverslips on PDMS mats. The samples were transferred onto SEM stubs adhered with double-sided carbon tape and sputter-coated with 20 nm of chromium (Quorum Q150T S).

FIB-SEM Imaging and Analysis. The samples as prepared above were imaged using an Auriga Zeiss Crossbeam FIB-SEM, using a 54° sample tilt and 36° image tilt correction at a working distance of 5 mm. Selected cells were coarse milled in part to reveal the inner structure at 2 nA:30 kV, after which SEM image stacks were acquired milling at 1 nA:30 kV with a 90 nm interval spacing at a 1.6 kV accelerating voltage using a backscattered electron detector. The obtained image stacks were automatically aligned using Fiji (ImageJ, StackReg plugin) and further finely manually aligned and segmented using Amira 5.3.2. (FEI).

Statistical Analysis. All experiments were performed as technical triplicate and three independent biological repeats ($n = 3$) unless otherwise stated. All data are presented as mean \pm standard deviation (SD) or as mean \pm standard error of the mean (SEM). One-way ANOVA was typically used for statistical analysis followed by a Bonferroni multiple comparison test (unless specified otherwise), using GraphPad Prism software version 8 ($ns\ p > 0.05$, $*p \leq 0.05$, $**p \leq 0.01$, $***p \leq 0.001$, $****p \leq 0.0001$).

ASSOCIATED CONTENT

Supporting Information

The Supporting Information is available free of charge at <https://pubs.acs.org/doi/10.1021/acsnano.0c04489>.

Supporting Figures 1–9 (effect of endocytic uptake inhibitors, physicochemical characterization data, additional FIB-SEM imaging data, impact of BMP lipid on

SP-B-mediated fusion and cellular delivery, and impact of bafilomycin A1 on SP-B-mediated intracellular delivery) (PDF)

FIB-SEM 3D reconstruction movie H1299_eGFP cell treated with LIP:AuNC (– SP-B) (ZIP)

FIB-SEM 3D reconstruction movie H1299_eGFP cell treated with LIP:AuNC (+ SP-B) (ZIP)

AUTHOR INFORMATION

Corresponding Author

Koen Raemdonck – Ghent Research Group on Nanomedicines, Laboratory of General Biochemistry and Physical Pharmacy, Faculty of Pharmaceutical Sciences, Ghent University, 9000 Ghent, Belgium; orcid.org/0000-0002-9807-4715; Email: koen.raemdonck@ugent.be

Authors

Roberta Guagliardo – Ghent Research Group on Nanomedicines, Laboratory of General Biochemistry and Physical Pharmacy, Faculty of Pharmaceutical Sciences, Ghent University, 9000 Ghent, Belgium; orcid.org/0000-0001-5385-5211

Lore Herman – Ghent Research Group on Nanomedicines, Laboratory of General Biochemistry and Physical Pharmacy, Faculty of Pharmaceutical Sciences, Ghent University, 9000 Ghent, Belgium

Jelle Penders – Department of Materials, Department of Bioengineering and Institute of Biomedical Engineering, Imperial College London, London SW7 2AZ, U.K.; orcid.org/0000-0002-5232-917X

Agata Zamborlin – Ghent Research Group on Nanomedicines, Laboratory of General Biochemistry and Physical Pharmacy, Faculty of Pharmaceutical Sciences, Ghent University, 9000 Ghent, Belgium

Herlinde De Keersmaecker – Ghent Research Group on Nanomedicines, Laboratory of General Biochemistry and Physical Pharmacy, Faculty of Pharmaceutical Sciences and Centre for Advanced Light Microscopy, Ghent University, 9000 Ghent, Belgium

Thijs Van de Vyver – Ghent Research Group on Nanomedicines, Laboratory of General Biochemistry and Physical Pharmacy, Faculty of Pharmaceutical Sciences, Ghent University, 9000 Ghent, Belgium; orcid.org/0000-0002-8030-6768

Sandrine Verstraeten – Université Catholique de Louvain, Louvain Drug Research Institute, Pharmacologie Cellulaire et Moléculaire, 1200 Brussels, Belgium

Pieterjan Merckx – Ghent Research Group on Nanomedicines, Laboratory of General Biochemistry and Physical Pharmacy, Faculty of Pharmaceutical Sciences, Ghent University, 9000 Ghent, Belgium; orcid.org/0000-0002-3274-6144

Marie-Paule Mingeot-Leclercq – Université Catholique de Louvain, Louvain Drug Research Institute, Pharmacologie Cellulaire et Moléculaire, 1200 Brussels, Belgium

Mercedes Echaide – Departamento de Bioquímica y Biología Molecular, Facultad de Biología, and Research Institute Hospital 12 de Octubre, Universidad Complutense, 28040 Madrid, Spain

Jesús Pérez-Gil – Departamento de Bioquímica y Biología Molecular, Facultad de Biología, and Research Institute Hospital 12 de Octubre, Universidad Complutense, 28040 Madrid, Spain

Molly M. Stevens – Department of Materials, Department of Bioengineering and Institute of Biomedical Engineering, Imperial College London, London SW7 2AZ, U.K.; orcid.org/0000-0002-7335-266X

Stefaan C. De Smedt – Ghent Research Group on Nanomedicines, Laboratory of General Biochemistry and Physical Pharmacy, Faculty of Pharmaceutical Sciences, Ghent University, 9000 Ghent, Belgium; orcid.org/0000-0002-8653-2598

Complete contact information is available at: <https://pubs.acs.org/10.1021/acsnano.0c04489>

Author Contributions

Conceptualization and study design: R.G., S.D.S., and K.R. Experimental work and data analysis: R.G., L.H., J.P., A.Z., H.D.K., T.V.d.V., S.V., P.M., and K.R. S.V. and M-P.M-L. contributed to the *in vitro* fusion data. J.P. and M.S. assisted with the FIB-SEM experiments and data analysis. M.E. and J.P.-G. provided the purified porcine SP-B. S.D.S. and K.R. supervised the study. The manuscript was written through contributions of all authors. All authors have given approval to the final version of the manuscript.

Notes

The authors declare no competing financial interest.

ACKNOWLEDGMENTS

R. Guagliardo, J. Penders, M. Stevens, S. De Smedt, and K. Raemdonck acknowledge NANOMED, which has received funding from the European Union's Horizon 2020 research and innovation program Marie Skłodowska Curie Innovative Training Networks (ITN) under grant no. 676137. R. Guagliardo additionally acknowledges Ghent University Special Research Fund (BOF19/ITN/001). A. Zamborlin acknowledges the Erasmus+ traineeship mobility program. H. De Keersmaecker acknowledges Ghent University (BO-FEXP2017001401). T. Van de Vyver, P. Merckx, and L. Herman are doctoral fellows of the Research Foundation-Flanders (grants 1198719N, 1S30616N, 1S56121N; FWO, Belgium). S. Verstraeten is a doctoral fellow of Télévie. M-P. Mingot-Leclercq acknowledges the Belgian Fonds de la Recherche Scientifique (FSR-FNRS T.003-14; J.0205.16; T.0175.20) and the Action de Recherche Concertée (ARC, UCL, 17-22-85). J. Pérez-Gil and M. Echaide acknowledge the support of grants from the Spanish Ministry of Science and Innovation (RTI2018-094564-B-I00) and the Regional Government of Madrid (P2018/NMT-4389). S. De Smedt and K. Raemdonck gratefully acknowledge Ghent University (BOF12/GOA/014, BOF19/GOA/008) and the Flanders Innovation & Entrepreneurship Agency (VLAIO SBO 140061). The authors gratefully acknowledge the technical assistance of Virginie Mohymont (Université Catholique de Louvain) and the Harvey Flower Micro Characterization Suite at the Department of Materials (Imperial College London), for their support.

REFERENCES

(1) Bartoszewski, R.; Sikorski, A. F. Editorial Focus: Understanding Off-Target Effects as the Key to Successful RNAi Therapy. *Cell. Mol. Biol. Lett.* **2019**, *24*, 69.
(2) Buyens, K.; Meyer, M.; Wagner, E.; Demeester, J.; De Smedt, S. C.; Sanders, N. N. Monitoring the Disassembly of SiRNA Polyplexes in Serum Is Crucial for Predicting Their Biological Efficacy. *J. Controlled Release* **2010**, *141*, 38–41.

(3) Dowdy, S. F. Overcoming Cellular Barriers for RNA Therapeutics. *Nat. Biotechnol.* **2017**, *35*, 222–229.

(4) Alagia, A.; Eritja, R. SiRNA and RNAi Optimization. *Wiley Interdiscip. Rev. RNA* **2016**, *7*, 316–329.

(5) Stewart, M. P.; Sharei, A.; Ding, X.; Sahay, G.; Langer, R.; Jensen, K. F. Break and Enter: *In Vitro* and *Ex Vivo* Strategies for Intracellular Delivery. *Nature* **2016**, *538*, 183–192.

(6) Yin, H.; Kanasty, R. L.; Eltoukhy, A. A.; Vegas, A. J.; Dorkin, J. R.; Anderson, D. G. Non-Viral Vectors for Gene-Based Therapy. *Nat. Rev. Genet.* **2014**, *15*, 541–555.

(7) Zinn, E.; Vandenberghe, L. H. Adeno-Associated Virus: Fit to Serve. *Curr. Opin. Virol.* **2014**, *8*, 90–97.

(8) Nidetz, N. F.; McGee, M. C.; Tse, L. V.; Li, C.; Cong, L.; Li, Y.; Huang, W. Adeno-Associated Viral Vector-Mediated Immune Responses: Understanding Barriers to Gene Delivery. *Pharmacol. Ther.* **2020**, *207*, 107453.

(9) Thomas, C. E.; Ehrhardt, A.; Kay, M. A. Progress and Problems with the Use of Viral Vectors for Gene Therapy. *Nat. Rev. Genet.* **2003**, *4*, 346–358.

(10) Akinc, A.; Maier, M. A.; Manoharan, M.; Fitzgerald, K.; Jayaraman, M.; Barros, S.; Ansell, S.; Du, X.; Hope, M. J.; Madden, T. D.; Mui, B. L.; Semple, S. C.; Tam, Y. K.; Ciufolini, M.; Witzigmann, D.; Kulkarni, J. A.; van der Meel, R.; Cullis, P. R. The Onpatro Story and the Clinical Translation of Nanomedicines Containing Nucleic Acid-Based Drugs. *Nat. Nanotechnol.* **2019**, *14*, 1084–1087.

(11) Stewart, M. P.; Lorenz, A.; Dahlman, J.; Sahay, G. Challenges in Carrier-Mediated Intracellular Delivery: Moving beyond Endosomal Barriers. *Wiley Interdiscip. Rev. Nanomedicine Nanobiotechnology* **2016**, *8*, 465–478.

(12) Iversen, T.-G. G.; Skotland, T.; Sandvig, K. Endocytosis and Intracellular Transport of Nanoparticles: Present Knowledge and Need for Future Studies. *Nano Today* **2011**, *6*, 176–185.

(13) Gilleron, J.; Querbes, W.; Zeigerer, A.; Borodovsky, A.; Marsico, G.; Schubert, U.; Manygoats, K.; Seifert, S.; Andree, C.; Stöter, M.; Epstein-Barash, H.; Zhang, L.; Kotliansky, V.; Fitzgerald, K.; Fava, E.; Bickle, M.; Kalaidzidis, Y.; Akinc, A.; Maier, M.; Zerial, M. Image-Based Analysis of Lipid Nanoparticle-Mediated SiRNA Delivery, Intracellular Trafficking and Endosomal Escape. *Nat. Biotechnol.* **2013**, *31*, 638–646.

(14) Sahay, G.; Querbes, W.; Alabi, C.; Eltoukhy, A.; Sarkar, S.; Zurenko, C.; Karagiannis, E.; Love, K.; Chen, D.; Zoncu, R.; Buganim, Y.; Schroeder, A.; Langer, R.; Anderson, D. G. Efficiency of SiRNA Delivery by Lipid Nanoparticles Is Limited by Endocytic Recycling. *Nat. Biotechnol.* **2013**, *31*, 653–658.

(15) De Backer, L.; Braeckmans, K.; Stuart, M. C. A.; Demeester, J.; De Smedt, S. C.; Raemdonck, K. Bio-Inspired Pulmonary Surfactant-Modified Nanogels: A Promising SiRNA Delivery System. *J. Controlled Release* **2015**, *206*, 177–186.

(16) De Backer, L.; Braeckmans, K.; Demeester, J.; De Smedt, S. C.; Raemdonck, K. The Influence of Natural Pulmonary Surfactant on the Efficacy of SiRNA-Loaded Dextran Nanogels. *Nanomedicine* **2013**, *8*, 1625–1638.

(17) De Backer, L.; Cerrada, A.; Pérez-Gil, J.; De Smedt, S. C.; Raemdonck, K. Bio-Inspired Materials in Drug Delivery: Exploring the Role of Pulmonary Surfactant in SiRNA Inhalation Therapy. *J. Controlled Release* **2015**, *220*, 642–650.

(18) De Backer, L.; Naessens, T.; De Koker, S.; Zagato, E.; Demeester, J.; Grooten, J.; De Smedt, S. C.; Raemdonck, K. Hybrid Pulmonary Surfactant-Coated Nanogels Mediate Efficient *In Vivo* Delivery of SiRNA to Murine Alveolar Macrophages. *J. Controlled Release* **2015**, *217*, 53–63.

(19) Merckx, P.; De Backer, L.; Van Hoecke, L.; Guagliardo, R.; Echaide, M.; Baatsen, P.; Olmeda, B.; Saelens, X.; Pérez-Gil, J.; De Smedt, S. C.; Raemdonck, K. Surfactant Protein B (SP-B) Enhances the Cellular SiRNA Delivery of Proteolipid Coated Nanogels for Inhalation Therapy. *Acta Biomater.* **2018**, *78*, 236–246.

(20) Guagliardo, R.; Merckx, P.; Zamborlin, A.; De Backer, L.; Echaide, M.; Pérez-Gil, J.; De Smedt, S. C.; Raemdonck, K. Nanocarrier Lipid Composition Modulates the Impact of Pulmonary

Surfactant Protein B (SP-B) on Cellular Delivery of siRNA. *Pharmaceutics* **2019**, *11*, 431.

(21) Echaide, M.; Autilio, C.; Arroyo, R.; Perez-Gil, J. Restoring Pulmonary Surfactant Membranes and Films at the Respiratory Surface. *Biochim. Biophys. Acta, Biomembr.* **2017**, *1859*, 1725–1739.

(22) Autilio, C.; Pérez-Gil, J. Understanding the Principle Biophysical Concepts of Pulmonary Surfactant in Health and Disease. *Arch. Dis. Child. - Fetal Neonatal Ed.* **2018**, *104*, F443–451.

(23) Guagliardo, R.; Pérez-Gil, J.; De Smedt, S.; Raemdonck, K. Pulmonary Surfactant and Drug Delivery: Focusing on the Role of Surfactant Proteins. *J. Controlled Release* **2018**, *291*, 116–126.

(24) Wright, J. R. Immunoregulatory Functions of Surfactant Proteins. *Nat. Rev. Immunol.* **2005**, *5*, 58–68.

(25) Arik, S.; Nishitani, C.; Kuroki, Y. Diverse Functions of Pulmonary Collectins in Host Defense of the Lung. *J. Biomed. Biotechnol.* **2012**, *2012*, 532071.

(26) Arias-Diaz, J.; Garcia-Verdugo, I.; Casals, C.; Sanchez-Rico, N.; Vara, E.; Balibrea, J. L. Effect of Surfactant Protein A (SP-A) on the Production of Cytokines by Human Pulmonary Macrophages. *Shock* **2000**, *14*, 300–306.

(27) Olmeda, B.; García-Álvarez, B.; Gómez, M. J.; Martínez-Calle, M.; Cruz, A.; Pérez-Gil, J.; Garcia-Álvarez, B.; Gomez, M. J.; Martinez-Calle, M.; Cruz, A.; Perez-Gil, J. A Model for the Structure and Mechanism of Action of Pulmonary Surfactant Protein B. *FASEB J.* **2015**, *29*, 4236–4247.

(28) Cabré, E. J.; Malmström, J.; Sutherland, D.; Pérez-Gil, J.; Otzen, D. E. Surfactant Protein SP-B Strongly Modifies Surface Collapse of Phospholipid Vesicles: Insights from a Quartz Crystal Microbalance with Dissipation. *Biophys. J.* **2009**, *97*, 768–776.

(29) Roldan, N.; Nyholm, T. K. M.; Slotte, J. P.; Pérez-Gil, J.; García-Álvarez, B. Effect of Lung Surfactant Protein SP-C and SP-C-Promoted Membrane Fragmentation on Cholesterol Dynamics. *Biophys. J.* **2016**, *111*, 1703–1713.

(30) Pérez-Gil, J. Structure of Pulmonary Surfactant Membranes and Films: The Role of Proteins and Lipid-Protein Interactions. *Biochim. Biophys. Acta, Biomembr.* **2008**, *1778*, 1676–1695.

(31) Obladen, M. History of Surfactant up to 1980. *Neonatology* **2005**, *87*, 308–316.

(32) Halliday, H. L. Surfactants: Past, Present and Future. *J. Perinatol.* **2008**, *28*, S47–S56.

(33) Halliday, H. L. History of Surfactant from 1980. *Neonatology* **2005**, *87*, 317–322.

(34) Hidalgo, A.; Cruz, A.; Pérez-Gil, J. Barrier or Carrier? Pulmonary Surfactant and Drug Delivery. *Eur. J. Pharm. Biopharm.* **2015**, *95*, 117–127.

(35) Kapralov, A. A.; Feng, W. H.; Amoscato, A. A.; Yanamala, N.; Balasubramanian, K.; Winnica, D. E.; Kisin, E. R.; Kotchey, G. P.; Gou, P.; Sparvero, L. J.; Ray, P.; Mallampalli, R. K.; Klein-Seetharaman, J.; Fadeel, B.; Star, A.; Shvedova, A. A.; Kagan, V. E. Adsorption of Surfactant Lipids by Single-Walled Carbon Nanotubes in Mouse Lung upon Pharyngeal Aspiration. *ACS Nano* **2012**, *6*, 4147–4156.

(36) Garcia-Mouton, C.; Hidalgo, A.; Cruz, A.; Pérez-Gil, J. The Lord of the Lungs: The Essential Role of Pulmonary Surfactant upon Inhalation of Nanoparticles. *Eur. J. Pharm. Biopharm.* **2019**, *144*, 230–243.

(37) Francia, V.; Yang, K.; Deville, S.; Reker-Smit, C.; Nelissen, I.; Salvati, A. Corona Composition Can Affect the Mechanisms Cells Use to Internalize Nanoparticles. *ACS Nano* **2019**, *13*, 11107–11121.

(38) Qiu, Y.; Chow, M. Y. T. T.; Liang, W.; Chung, W. W. Y. Y.; Mak, J. C. W. W.; Lam, J. K. W. W. From Pulmonary Surfactant, Synthetic KL4 Peptide as Effective siRNA Delivery Vector for Pulmonary Delivery. *Mol. Pharmaceutics* **2017**, *14*, 4606–4617.

(39) Witttrup, A.; Ai, A.; Liu, X.; Hamar, P.; Trifonova, R.; Charisse, K.; Manoharan, M.; Kirchhausen, T.; Lieberman, J. Visualizing Lipid-Formulated siRNA Release from Endosomes and Target Gene Knockdown. *Nat. Biotechnol.* **2015**, *33*, 870–876.

(40) Vermeulen, L. M. P.; Brans, T.; Samal, S. K.; Dubruel, P.; Demeester, J.; De Smedt, S. C.; Remaut, K.; Braeckmans, K.

Endosomal Size and Membrane Leakiness Influence Proton Sponge-Based Rupture of Endosomal Vesicles. *ACS Nano* **2018**, *12*, 2332–2345.

(41) Rehman, Z. U.; Hoekstra, D.; Zuhorn, I. S. Mechanism of Polyplex- and Lipoplex-Mediated Delivery of Nucleic Acids: Real-Time Visualization of Transient Membrane Destabilization without Endosomal Lysis. *ACS Nano* **2013**, *7*, 3767–3777.

(42) Van de Vyver, T.; Bogaert, B.; De Backer, L.; Joris, F.; Guagliardo, R.; Van Hoeck, J.; Merckx, P.; Van Calenbergh, S.; Ramishetti, S.; Peer, D.; Remaut, K.; De Smedt, S. C.; Raemdonck, K. Cationic Amphiphilic Drugs Boost the Lysosomal Escape of Small Nucleic Acid Therapeutics in a Nanocarrier-Dependent Manner. *ACS Nano* **2020**, *14*, 4791.

(43) Wolfson, M. R.; Wu, J.; Hubert, T. L.; Gregory, T. J.; Mazela, J.; Shaffer, T. H. Lucinactant Attenuates Pulmonary Inflammatory Response, Preserves Lung Structure, and Improves Physiologic Outcomes in a Preterm Lamb Model of RDS. *Pediatr. Res.* **2012**, *72*, 375–383.

(44) Braide-Moncoeur, O.; Tran, N. T.; Long, J. R. Peptide-Based Synthetic Pulmonary Surfactant for the Treatment of Respiratory Distress Disorders. *Curr. Opin. Chem. Biol.* **2016**, *32*, 22–28.

(45) European Medicines Agency. *Withdrawal Public Assessment Report of the Marketing Authorisation Application for Surfaxin (Sinapultide, Dipalmitoylphosphatidylcholine, Palmitoyl-Oleoyl Phosphatidylglycerol, Palmitic Acid)*; 2006; October, pp 1–25.

(46) Charatan, F. Surfactant Trial in Latin American Infants Criticised. *BMJ* **2001**, *322*, 575.

(47) Hentschel, R.; Bohlin, K.; van Kaam, A.; Fuchs, H.; Danhaive, O. Surfactant Replacement Therapy: From Biological Basis to Current Clinical Practice. *Pediatr. Res.* **2020**, *88*, 176–183.

(48) Qiu, Y.; Man, R. C. H.; Liao, Q.; Kung, K. L. K.; Chow, M. Y. T.; Lam, J. K. W. Effective mRNA Pulmonary Delivery by Dry Powder Formulation of PEGylated Synthetic KL4 Peptide. *J. Controlled Release* **2019**, *314*, 102–115.

(49) Martínez-Calle, M.; Olmeda, B.; Dietl, P.; Frick, M.; Pérez-Gil, J. Pulmonary Surfactant Protein SP-B Promotes Exocytosis of Lamellar Bodies in Alveolar Type II Cells. *FASEB J.* **2018**, *32*, 4600–4611.

(50) Ryan, M. A.; Qi, X.; Serrano, A. G.; Ikegami, M.; Perez-Gil, J.; Johansson, J.; Weaver, T. E. Mapping and Analysis of the Lytic and Fusogenic Domains of Surfactant Protein B. *Biochemistry* **2005**, *44*, 861–872.

(51) Naeye, B.; Deschout, H.; Cavelliers, V.; Descamps, B.; Braeckmans, K.; Vanhove, C.; Demeester, J.; Lahoutte, T.; De Smedt, S. C.; Raemdonck, K. *In Vivo* Disassembly of IV Administered siRNA Matrix Nanoparticles at the Renal Filtration Barrier. *Biomaterials* **2013**, *34*, 2350–2358.

(52) Guehrs, E.; Schneider, M.; Günther, C. M.; Hensing, P.; Heitz, K.; Wittke, D.; López-Serrano Oliver, A.; Jakubowski, N.; Plendl, J.; Eisebitt, S.; Haase, A. Quantification of Silver Nanoparticle Uptake and Distribution within Individual Human Macrophages by FIB/SEM Slice and View. *J. Nanobiotechnol.* **2017**, *15*, 21.

(53) Vermeulen, L. M. P.; Brans, T.; De Smedt, S. C.; Remaut, K.; Braeckmans, K. Methodologies to Investigate Intracellular Barriers for Nucleic Acid Delivery in Non-Viral Gene Therapy. *Nano Today* **2018**, *21*, 74–90.

(54) Kauscher, U.; Penders, J.; Nagelkerke, A.; Holme, M. N.; Nele, V.; Massi, L.; Gopal, S.; Whittaker, T. E.; Stevens, M. M. Gold Nanocluster Extracellular Vesicle Supraparticles: Self-Assembled Nanostructures for Three-Dimensional Uptake Visualization. *Langmuir* **2020**, *36*, 3912–3923.

(55) Baoukina, S.; Tieleman, D. P. Lung Surfactant Protein SP-B Promotes Formation of Bilayer Reservoirs from Monolayer and Lipid Transfer between the Interface and Subphase. *Biophys. J.* **2011**, *100*, 1678–1687.

(56) Cabre, E. J.; Martínez-Calle, M.; Prieto, M.; Fedorov, A.; Olmeda, B.; Loura, L. M. S.; Perez-Gil, J. Homo- and Hetero-Oligomerization of Hydrophobic Pulmonary Surfactant Proteins SP-B

and SP-C in Surfactant Phospholipid Membranes. *J. Biol. Chem.* **2018**, 2939399

(57) Hoekstra, D.; de Boer, T.; Klappe, K.; Wilschut, J. Fluorescence Method for Measuring the Kinetics of Fusion between Biological Membranes. *Biochemistry* **1984**, 23, 5675–5681.

(58) Nunes-Correia, L.; Eulálio, A.; Nir, S.; Düzgünes, N.; Ramalho-Santos, J.; Pedroso De Lima, M. C. Fluorescent Probes for Monitoring Virus Fusion Kinetics: Comparative Evaluation of Reliability. *Biochim. Biophys. Acta, Biomembr.* **2002**, 1561, 65–75.

(59) Triakash, I.; Gumenyuk, V.; Lishko, V. The Fusion of Synaptic Vesicle Membranes Studied by Lipid Mixing: The R18 Fluorescence Assay Validity. *Chem. Phys. Lipids* **2010**, 163, 778–786.

(60) Erazo-Oliveras, A.; Najjar, K.; Truong, D.; Wang, T. Y.; Brock, D. J.; Prater, A. R.; Pellois, J. P. The Late Endosome and Its Lipid BMP Act as Gateways for Efficient Cytosolic Access of the Delivery Agent DfTAT and Its Macromolecular Cargos. *Cell Chem. Biol.* **2016**, 23, 598–607.

(61) Oosterlaken-Dijksterhuis, M. A.; van Eijk, M.; van Golde, L. M. G.; Haagsman, H. P. Lipid Mixing Is Mediated by the Hydrophobic Surfactant Protein SP-B but Not by SP-C. *Biochim. Biophys. Acta, Biomembr.* **1992**, 1110, 45–50.

(62) Gruenberg, J. Life in the Lumen: The Multivesicular Endosome. *Traffic* **2019**, 21, 12715.

(63) Cabre, E. J.; Martinez-Calle, M.; Prieto, M.; Fedorov, A.; Olmeda, B.; Loura, L. M. S. L. M. S.; Perez-Gil, J.; Martnez-Calle, M.; Prieto, M.; Fedorov, A.; Olmeda, B.; Loura, L. M. S. L. M. S.; Perez-Gil, J. Homo- A Nd Hetero-Oligomerization of Hydrophobic Pulmonary Surfactant Proteins SP-B and SP-C in Surfactant Phospholipid Membranes. *J. Biol. Chem.* **2018**, 293, 9399–9411.

(64) Cabré, E. J.; Loura, L. M. S.; Fedorov, A.; Perez-Gil, J.; Prieto, M. Topology and Lipid Selectivity of Pulmonary Surfactant Protein SP-B in Membranes: Answers from Fluorescence. *Biochim. Biophys. Acta, Biomembr.* **2012**, 1818, 1717–1725.

(65) Liekkinen, J.; Enkavi, G.; Javanainen, M.; Olmeda, B.; Pérez-Gil, J.; Vattulainen, I. Pulmonary Surfactant Lipid Reorganization Induced by the Adsorption of the Oligomeric Surfactant Protein B Complex. *J. Mol. Biol.* **2020**, 432, 3251–3268.

(66) Ryan, M. A.; Akinbi, H. T.; Serrano, A. G.; Perez-Gil, J.; Wu, H.; McCormack, F. X.; Weaver, T. E. Antimicrobial Activity of Native and Synthetic Surfactant Protein B Peptides. *J. Immunol.* **2006**, 176, 416–425.

(67) Hawgood, S.; Derrick, M.; Poulain, F. Structure and Properties of Surfactant Protein B. *Biochim. Biophys. Acta, Mol. Basis Dis.* **1998**, 1408, 150–160.

(68) Longo, M. L.; Bisagno, A. M.; Zasadzinski, J. A. N.; Bruni, R.; Waring, A. J. A Function of Lung Surfactant Protein SP-B. *Science* **1993**, 261, 453–456.

(69) Olmeda, B.; Martínez-Calle, M.; Pérez-Gil, J. Pulmonary Surfactant Metabolism in the Alveolar Airspace: Biogenesis, Extracellular Conversions, Recycling. *Ann. Anat.* **2017**, 209, 78–92.

(70) Litvinov, D. Y.; Savushkin, E. V.; Dergunov, A. D. Intracellular and Plasma Membrane Events in Cholesterol Transport and Homeostasis. *J. Lipids* **2018**, 2018, 1–22.

(71) Van Meer, G.; Voelker, D. R.; Feigenson, G. W. Membrane Lipids: Where They Are and How They Behave. *Nat. Rev. Mol. Cell Biol.* **2008**, 9, 112–124.

(72) Rivel, T.; Ramseyer, C.; Yesylevskyy, S. The Asymmetry of Plasma Membranes and Their Cholesterol Content Influence the Uptake of Cisplatin. *Sci. Rep.* **2019**, 9, 5627.

(73) Huotari, J.; Helenius, A. Endosome Maturation. *EMBO J.* **2011**, 30, 3481–3500.

(74) Bissig, C.; Gruenberg, J. Lipid Sorting and Multivesicular Endosome Biogenesis. *Cold Spring Harb Perspect Biol.* **2013**, 5, No. a016816.

(75) Gruenberg, J.; Van Der Goot, F. G. Mechanisms of Pathogen Entry through the Endosomal Compartments. *Nat. Rev. Mol. Cell Biol.* **2006**, 7, 495–504.

(76) Zaitseva, E.; Yang, S. T.; Melikov, K.; Pourmal, S.; Chernomordik, L. V. Dengue Virus Ensures Its Fusion in Late

Endosomes Using Compartment-Specific Lipids. *PLoS Pathog.* **2010**, 6, No. e1001131.

(77) Bitto, D.; Halldorsson, S.; Caputo, A.; Huiskonen, J. T. Low PH and Anionic Lipid-Dependent Fusion of Uukuniemi Phlebovirus to Liposomes. *J. Biol. Chem.* **2016**, 291, 6412–6422.

(78) Matos, P. M.; Marin, M.; Ahn, B.; Lam, W.; Santos, N. C.; Melikyan, G. B. Anionic Lipids Are Required for Vesicular Stomatitis Virus G Protein-Mediated Single Particle Fusion with Supported Lipid Bilayers. *J. Biol. Chem.* **2013**, 288, 12416–12425.

(79) White, J. M.; Whittaker, G. R. Fusion of Enveloped Viruses in Endosomes. *Traffic* **2016**, 17, 593–614.

(80) Shi, G.; Ozog, S.; Torbett, B. E.; Compton, A. A. MTOR Inhibitors Lower an Intrinsic Barrier to Virus Infection Mediated by IFITM3. *Proc. Natl. Acad. Sci. U. S. A.* **2018**, 115, E10069–E10078.

(81) Record, M.; Silvente-Poirot, S.; Poirot, M.; Wakelam, M. J. O. Extracellular Vesicles: Lipids as Key Components of Their Biogenesis and Functions. *J. Lipid Res.* **2018**, 59, 1316–1324.

(82) Olmeda, B.; García-Álvarez, B.; Pérez-Gil, J. Structure-Function Correlations of Pulmonary Surfactant Protein SP-B and the Saposin-Like Family of Proteins. *Eur. Biophys. J.* **2013**, 42, 209–222.

(83) Wilder, M. A. Surfactant Protein B Deficiency in Infants with Respiratory Failure. *J. Perinat Neonatal Nurs* **2004**, 18, 61–67.

(84) Johansson, J.; Curstedt, T. Synthetic Surfactants with SP-B and SP-C Analogues to Enable Worldwide Treatment of Neonatal Respiratory Distress Syndrome and Other Lung Diseases. *J. Intern. Med.* **2019**, 285, 165–186.

(85) Raemdonck, K.; Braeckmans, K.; Demeester, J.; De Smedt, S. C. Merging the Best of Both Worlds: Hybrid Lipid-Enveloped Matrix Nanocomposites in Drug Delivery. *Chem. Soc. Rev.* **2014**, 43, 444–472.

(86) van Dijk-Wolthuis, W. N. E.; Tsang, S. K. Y.; den Bosch, K. W. E.; Hennink, J. J. A New Class of Polymerizable Dextrans with Hydrolyzable Groups: Hydroxyethyl Methacrylated Dextran with and without Oligolactate Spacer. *Polymer* **2002**, 38, 6235–6242.

(87) van Dijk-Wolthuis, W. N. E.; Franssen, O.; Talsma, H.; van Steenberg, M. J.; Kettenes-Van den Bosch, J. J.; Hennink, W. E.; van Dijk-Wolthuis, W. N. E.; Franssen, O.; Talsma, H.; van Steenberg, M. J.; Kettenes-Van den Bosch, J. J.; Hennink, W. E. Synthesis, Characterization, and Polymerization of Glycidyl Methacrylate Derivatized Dextran. *Macromolecules* **1995**, 28, 6317–6322.

(88) Van Dijk-Wolthuis, W. N. E.; Kettenes-Van Den Bosch, J. J.; Van Der Kerk-Van Hoof, A.; Hennink, W. E. Reaction of Dextran with Glycidyl Methacrylate: An Unexpected Transesterification. *Macromolecules* **1997**, 30, 3411–3413.

SUPPORTING INFORMATION

Surfactant Protein B Promotes Cytosolic SiRNA Delivery by Adopting a Virus-like Mechanism of Action

Roberta Guagliardo¹, Lore Herman¹, Jelle Penders², Agata Zamborlin¹, Herlinde De Keersmaecker^{1,3}, Thijs Van de Vyver¹, Sandrine Verstraeten⁴, Pieterjan Merckx¹, Marie-Paule Mingeot-Leclercq⁴, Mercedes Echaide⁵, Jesús Pérez-Gil⁵, Molly M. Stevens², Stefaan C. De Smedt¹, Koen Raemdonck^{1}*

*Correspondence: koen.raemdonck@ugent.be

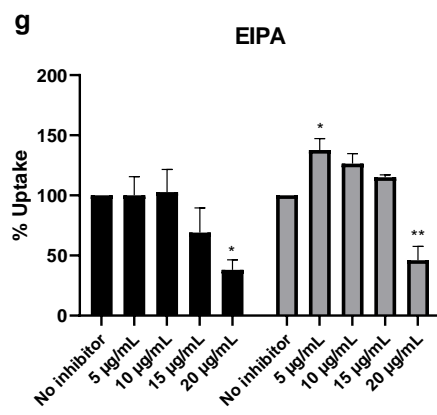
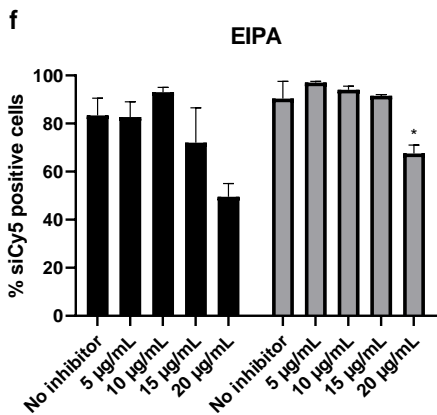
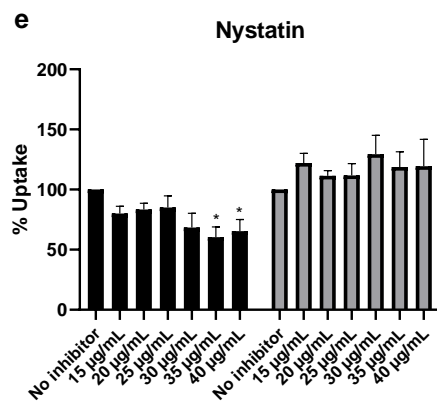
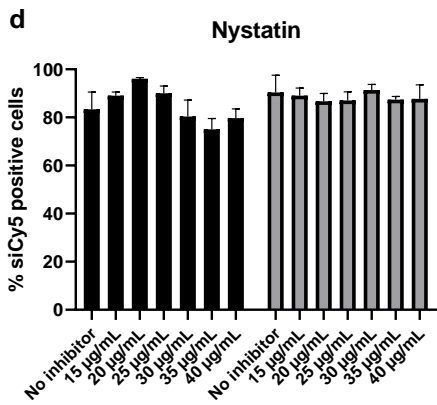
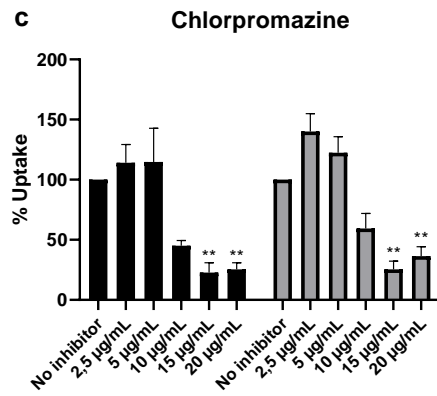
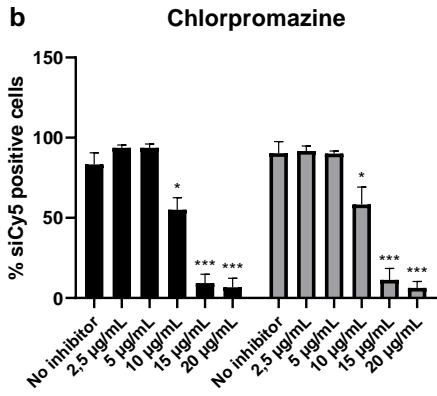
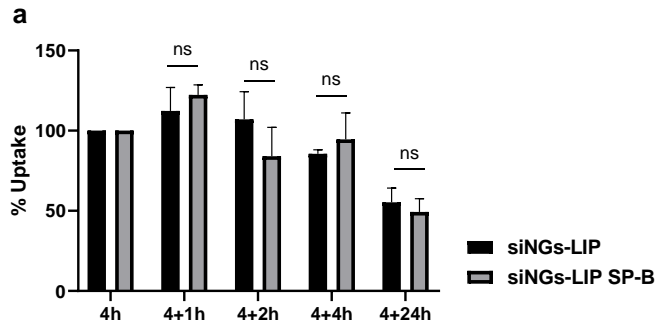
1. Ghent Research Group on Nanomedicines, Laboratory of General Biochemistry and Physical Pharmacy, Faculty of Pharmaceutical Sciences, Ghent University, Ottergemsesteenweg 460, 9000 Ghent, Belgium.

2. Department of Materials, Department of Bioengineering and Institute of Biomedical Engineering, Imperial College London, London SW7 2AZ, UK.

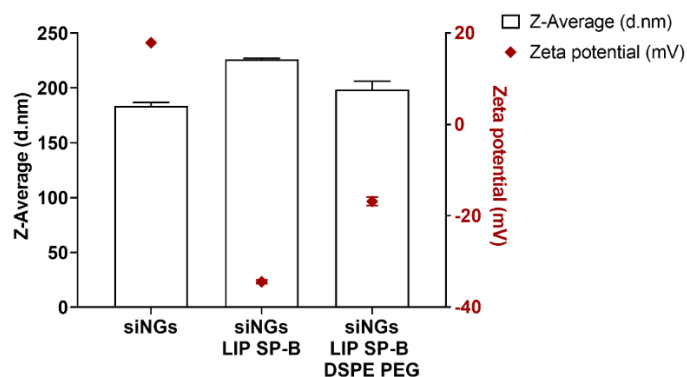
3. Centre for Advanced Light Microscopy, Ghent University, 9000 Ghent, Belgium.

4. Université Catholique de Louvain, Louvain Drug Research Institute, Pharmacologie Cellulaire et Moléculaire, Avenue E. Mounier 73, UCL B1.73.05, 1200 Brussels, Belgium.

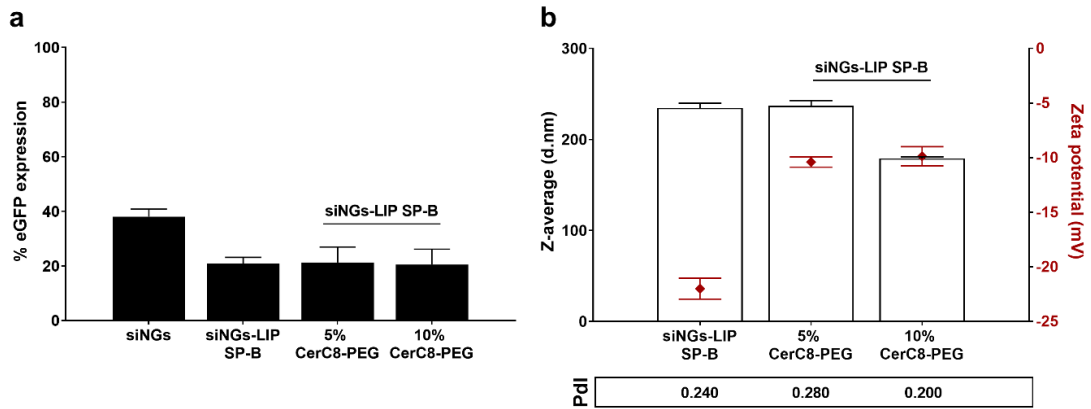
5. Departamento de Bioquímica y Biología Molecular, Facultad de Biología, and Research Institute Hospital 12 de Octubre, Universidad Complutense, José Antonio Novais 12, 28040 Madrid, Spain.



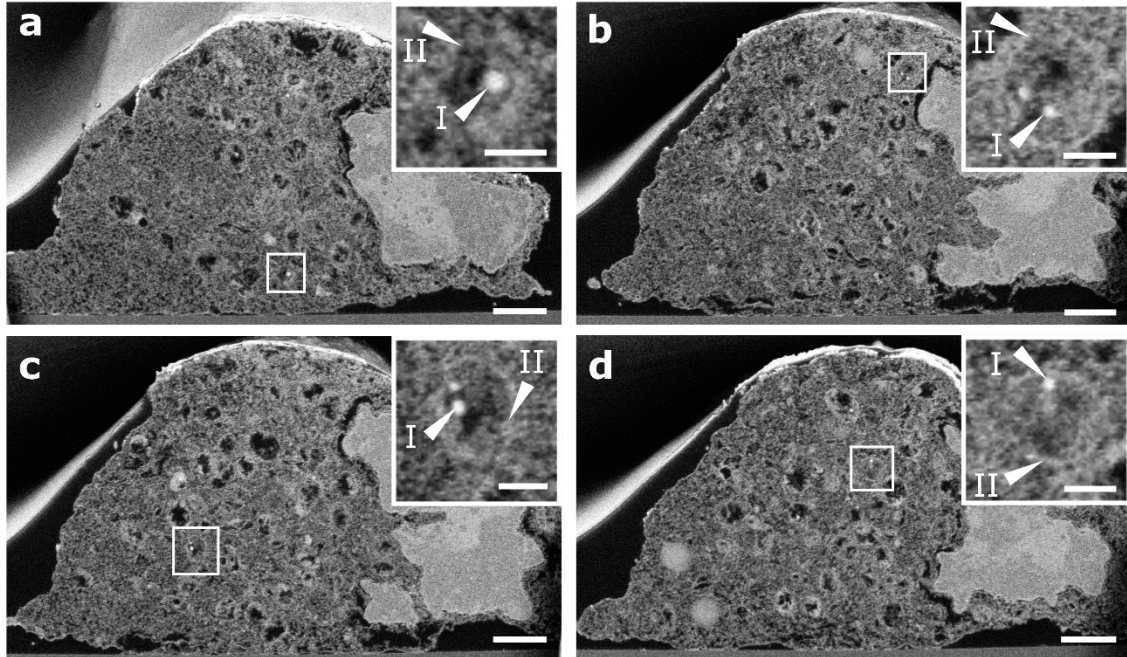
Supporting Figure 1. (a) Uptake of siNG-LIP and siNG-LIP SP-B (complexing Cy5-labeled siRNA (siCy5)) in H1299_eGFP cells, as quantified *via* flow cytometry at different time points post-transfection. Data are shown as a mean \pm SEM of three independent experiments. An unpaired *t* test was used for statistical analysis per time point, using GraphPad Prism software version 8 (ns $p > 0.05$). (b, d, f) Percentage siCy5 positive cells and (c, e, g) siCy5 uptake after pre- and co-incubation of H1299_eGFP cells with mounting concentrations of endocytic uptake inhibitors and siNG-LIP or siNG-LIP SP-B. Chlorpromazine, nystatin and 5-(*N*-ethyl-*N*-isopropyl)amiloride (EIPA) are inhibitors of clathrin-mediated endocytosis, caveolae-mediated endocytosis and macropinocytosis, respectively. Data are shown as mean \pm SEM of three independent experiments. One-way ANOVA with Dunnett's multiple comparisons test was used for statistical analysis, using GraphPad Prism software version 8 (* $p \leq 0.05$, ** $p \leq 0.01$, *** $p \leq 0.001$).



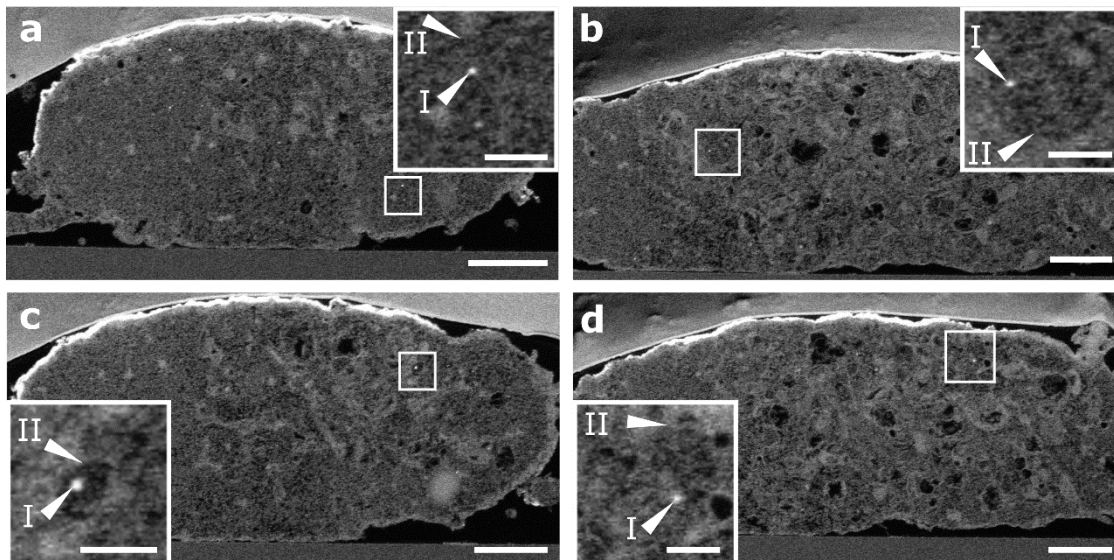
Supporting Figure 2. Hydrodynamic diameter and zeta potential of siRNA-loaded nanogels (siNGs) vs DOPC:PG (85:15 wt%) (proteo)lipid-coated siRNA-loaded nanogels (siNGs-LIP). Successful PEGylation of the lipid bilayer by insertion of DSPE-PEG₂₀₀₀ (10 wt%) is confirmed by the increase in the zeta potential of the ‘siNGs-LIP SP-B DSPE PEG’, compared to the ‘siNGs-LIP SP-B’.



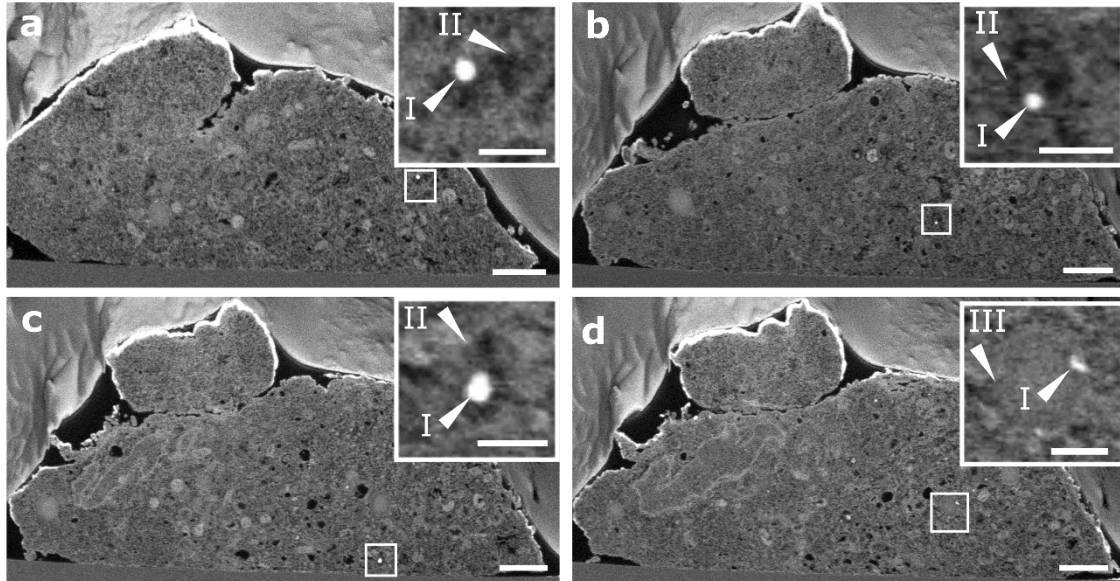
Supporting Figure 3. (a) Impact of reversible PEGylation on the gene silencing potential of siNGs-LIP SP-B (1 wt %) in H1299_eGFP cells, quantified *via* flow cytometry. (b) Size and zeta potential of siNGs-LIP SP-B (1 wt %) with or without CerC8-PEG. Successful PEGylation of the lipid coating is confirmed by the increase in zeta potential. Data are shown as a mean \pm SD of a technical triplicate.



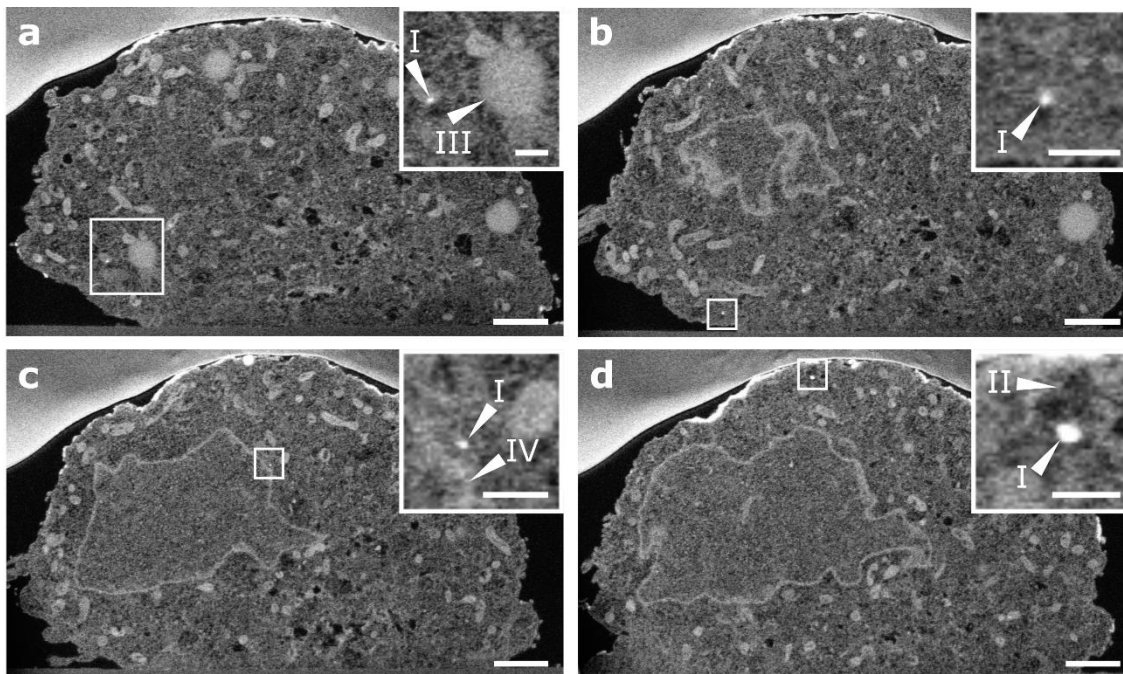
Supporting Figure 4. Additional FIB-SEM imaging showing presence in endosomes of DOPC:PG 85:15 wt% liposomes (LIP) without SP-B, with membrane-embedded gold nanoclusters (AuNCs) in H1299_eGFP cells after 2 hours of incubation. Close-ups in the insets showing regions of interest with the particles (I) and endosomal membranes (II) indicated. Scale bars = 2 μm in the main images and 500 nm in the insets.



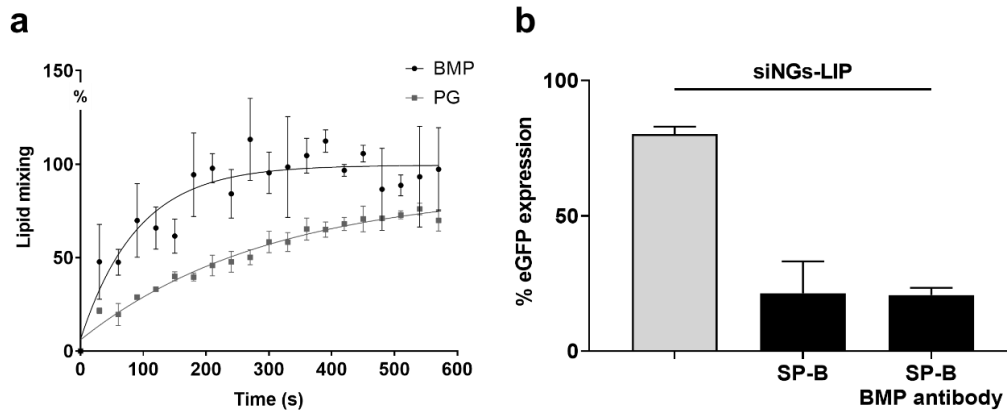
Supporting Figure 5. Additional FIB-SEM imaging showing presence in endosomes of DOPC:PG 85:15 wt% liposomes (LIP) with 0.4 wt.% SP-B with membrane-embedded gold nanoclusters (AuNCs) in H1299_eGFP cells after 2 hours of incubation. Close-ups in the insets showing regions of interest with the particles (I) and endosomal membranes (II) indicated. Scale bars = 2 μm in the main images and 500 nm in the insets.



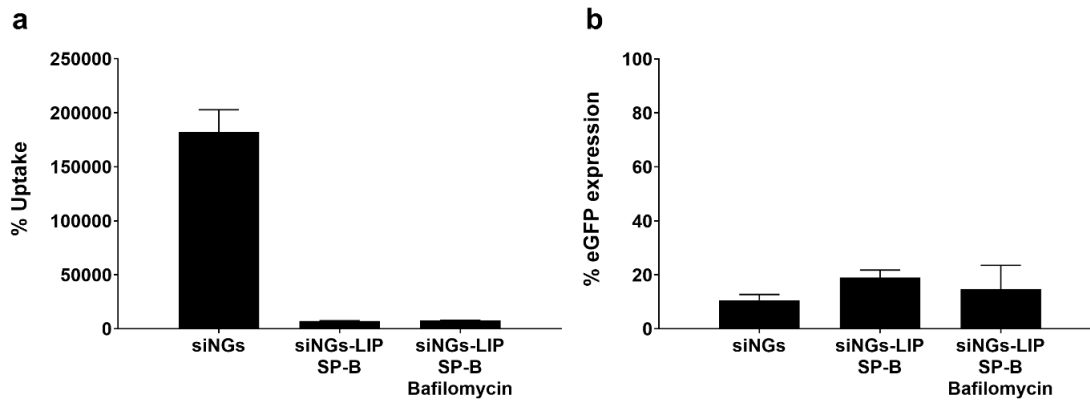
Supporting Figure 6. Additional FIB-SEM imaging showing presence in endosomes of DOPC:PG 85:15 wt% liposomes (LIP) without SP-B, with membrane-embedded gold nanoclusters (AuNCs) in H1299_eGFP cells after 4 hours of incubation. Close-ups in the insets showing regions of interest with the particles (I), endosomal membranes (II) and lysosomal membrane (III) indicated. Scale bars = 2 μm in the main images and 500 nm in the insets. A 3D reconstruction movie of this cell is available as Web Enhanced Object ‘Guagliardo *et al.* 2021 - SI movie 1- DOPC:PG 4h reconstruction’.



Supporting Figure 7. Additional FIB-SEM imaging showing presence in endosomes of DOPC:PG 85:15 wt% liposomes (LIP) with 0.4 wt% SP-B with membrane-embedded gold nanoclusters (AuNCs) in H1299_eGFP cells after 4 hours of incubation. Close-ups in the insets showing regions of interest with the particles (I), endosomal membranes (II), lysosomal membrane (III) and nuclear membrane (IV) indicated. Scale bars = 2 μm in the main images and 500 nm in the insets. A 3D reconstruction movie of this cell is available as Web Enhanced Object ‘Guagliardo *et al.* 2021 - SI movie 2- DOPC:PG:SPB 4h reconstruction’.



Supporting Figure 8. (a) Lipid mixing of SP-B containing liposomes with vesicles mimicking ILVs composed of BMP:PC:PE or PG:PC:PE (77:19:4 mol%) and 5.7 mol% of R18. (b) Evaluation of the impact of overnight pre-incubation with a BMP targeting antibody (50 μ g/mL) on the gene silencing potential of siNGs-LIP SP-B. Data are shown as a mean \pm SD of a technical triplicate.



Supporting Figure 9. (a) Flow cytometric quantification of siCy5 cellular uptake and (b) gene silencing of (un)coated formulations. Impact of bafilomycin treatment on SP-B mediated intracellular delivery. H1299_eGFP cells were pre-incubated with bafilomycin A1 (InvivoGen) (1.25 μ M) for 30 minutes and co-incubated with the siNGs-LIP SP-B for 4 hours. Data are shown as a mean \pm SD of a technical triplicate.